

JUACEP Program 2023 at UCLA, NCSU & PolyMTL



Japan-US-Canada Collaborative Education Program

Nagoya University

Table of Contents

<1> About the Program

1-1. Overview.....	4
1-2. Participants.....	5

<2> Research Reports and Presentations

Posters of the 31 st and 32 nd JUACEP Workshop.....	8
2-1. 2023 Medium-term course at Polytechnique Montréal Yu-Hsin Wu	9
2-2. 2023 Medium-term course at UCLA and NCSU Koyo Ueno_1	10
Koyo Ueno_2.....	17
Kaito Usami.....	21

<3> Findings through JUACEP

3-1. Students' reviews	32
3-2. Questionnaires (in Japanese).....	35

<1> About the Program

1-1. Overview ...P.4

1-2. Participants ...P.5



1-1. Overview

Nagoya University's JUACEP provides two course options for students at the Graduate School of Engineering to study abroad: the medium-term (up to seven months) course and the long-term (more than eight months) course. Choosing one of those courses, the selected students are offered an opportunity to work together with faculty and other researchers or students from all over the world at the world's top universities.

Each student works on a research project related to his own field's topic while belonging to a specialized research group of the partner universities in the United States or Canada. As of 2023, Partners are University of Michigan (UM), University of California, Los Angeles (UCLA), University of Toronto (UT), North Carolina State University (NCSU) and Polytechnique Montréal (PolyMTL).

In addition to research implementation, the students are expected to attend seminars, group discussions and other events. At the end of each course, the students are required to submit research reports to their mentors at the host institution, and after returning to Nagoya, give research presentations based on their achievements in front of the faculty and peer students at JUACEP Workshop held in Nagoya University. The report and the presentation are primary requisites to be accredited for the program completion.

This publication is compiling the activities of the following students.

[a] One student of medium-term course from July to October 2023 at Polytechnique Montréal.

[b] Two students of medium-term course from August 2023 to April 2024 at NCSU or UCLA.

JUACEP outbound 2023 Medium-term Course Flowchart

	[a] Medium-term course 2023 at POLYMTL	[b] Medium-term course 2023 at NCSU and UCLA
January 2023	Apply to POLY	
February	Accepted the screening result	
March	Prepare for the staying qualification	Approach to UCLA faculty and accepted
May		Prepare for *DS-2019/ J-1 visa
June		
July	Leave Japan for Canada and start the program	
August		Leave Japan for the US and start the program
September	Return to Japan Achievement presentation 31st Workshop, Oct. 18, 2023	
October		
March 2024		Return to Japan
April		Achievement presentation 32nd Workshop, April. 18, 2024

*DS-2019: Certificate of eligibility for Exchange Visitor Status

1-2. Participants

★Medium-term course at Polytechnique Montréal

Program period: June 3 - October 2, 2023

1	Yu-Hsin WU ウ ユシン	D2	Supervisor at PolyMTL: Assist.Prof. Antoine LESAGE-LANDRY, Electrical Engineering	Supervisor at NU: Prof. Masayoshi YAMAMOTO, Electrical Engineering
---	---------------------	----	---	--

★Medium-term course at NCSU

Program period: August 18, 2023 - April 5, 2024

2	Kaito USAMI 宇佐見 海渡	M1	Supervisor at NCSU: Assist.Prof. Chi-An YEA, Aerospace Engineering	Supervisor at NU: Assoc.Prof. Takaya INAMORI, Aerospace Engineering
---	-----------------------	----	--	---

★Medium-term course at UCLA

Program period: September 14, 2023 - March 31, 2024

3	Koyo UENO 上野 弘陽	M1	Supervisor at UCLA: Prof. Bruce DUNN, Materials Science	Supervisor at NU: Prof. Kazuki NAKANISHI, Materials Chemistry
---	--------------------	----	--	---

Coordinator

PolyMTL	Ms. Julie Defretin Strategic advisor, Internationalisation delphine.julen@polymtl.ca
NCSU	Mr. Tomohisa Koyama NCSU Coordinator and NU Representative in NC tkoyama@tpnu.org
UCLA	Prof. Jenn-Ming Yang Materials Science and Engineering jyang@seas.ucla.edu

JUACEP Committee and Advisory Members

Prof. Noritsugu Umehara	noritsugu.umehara@mae.nagoya-u.ac.jp	Office: 052-789-2785
Prof. Toshiro Matsumoto	matsumoto.toshiro.e6@f.mail.nagoya-u.ac.jp	Office: 052-789-2780
Prof. Yasumasa Ito	ito.yasumasa.y3@f.mail.nagoya-u.ac.jp	Office: 052-789-4488
Assoc. Prof. Takayuki Tokoroyama	takayuki.tokoroyama@mae.nagoya-u.ac.jp	Office: 052-789-2787
Assoc. Prof. Reiko Furuya	furuya.reiko.n5@f.mail.nagoya-u.ac.jp	Office: 052-789-3603
Assoc. Prof. Emanuel Leleito	leleito@nagoya-u.jp	Office: 052-789-3101
Assoc. Prof. Dina Grib	grib@nagoya-u.jp	Office: 052-789-3179
Tomoko Kato, Administrative staff	kato.tomoko.e6@f.mail.nagoya-u.ac.jp	Office: 052-789-2799

JUACEP Office

Rm #341, Engineering Building II, Nagoya University, Nagoya 4648603, Aichi
Tel/Fax +81 (0)52 789 2799, office@juacep.engg.nagoya-u.ac.jp

<2> Research Reports and Presentations

2-1. 2023 Medium-term course at Polytechnique Montréal, October - June 2023

Presentation at the 31st JUACEP Workshop, October 18, 2023

[Research Report]

Yu-Hsin Wu

“Combinational Optimization for Geospatial Wind Turbine Placement”
(Undisclosed) ...P.9

2-2. 2023 Medium-term course at North Carolina State University and University of California, Los Angeles, August 2023 - April 2024

Presentations at the 32nd JUACEP Workshop, April 18, 2024

[Presentations and Research Reports]

Koyo Ueno

“Pseudocapacitance of T-Nb₂O₅ Nanoparticles” ...P.10

“Investigation of Ionic Conductivity of Ionogel Electrolyte on Separator”
...P.17

Kaito Usami

“On the Frequency Lock-on within a Network of Oscillators Using
Phase-Reduction Analysis” ...P.21

The 31st JUACEP Workshop

2023 Summer Research Internship at Polytechnique Montréal

9:00 ~ 9:20 October 18, 2023

Venue: Knowledge Commons, 6F, C-TECs



* We would appreciate it if you register beforehand but feel free to just drop by any time without registration as well.

9:00 - 9:12 Presentation by Yu-Hsin WU on COMBINATORIAL OPTIMIZATION FOR GEOSPATIAL WIND TURBINE PLACEMENT and study abroad experience in Canada.
Advisor at NU Professor Masayoshi Yamamoto, Institute of Materials and Systems for Sustainability Center for Integrated Research of Future Electronics Division.
9:12 - 9:20 Q&A session and Completion ceremony

* We invite the prospective JUACEP participants and engineering students interested in studying abroad to participate and ask any questions related to the program.



Japan-US-Canada Advanced
Collaborative Education program
052-789-2799 JUACEP Office
<https://www.juacep.engg.nagoya-u.ac.jp/>



The 32nd JUACEP Workshop

2023 Outbound Course at UCLA & NC State University

15:00 - 15:45 April 18, 2024

Venue: 221, Engineering bldg.#2

(221講義室工学部2号館2階中央廊下)



* We would appreciate it if you register beforehand but feel free to just drop by any time without registration as well.

15:00 - 15:05 Opening Address
15:05 - 15:20 Presentation by **Koyo Ueno** on "Investigation of Ionic Conductivity of Ionogel Electrolyte on Separator" & "Pseudocapacitance of T-Nb2O5 Nanoparticles"
Advisor at NU: Professor Kazuki Nakanishi Dept. Materials Chemistry
15:20 - 15:35 Presentation by **Kaito Usami** on "Estimation for Multiple Oscillators' Global Coupling by Phase-Reduction Analysis"
Advisor at NU: Assoc. Professor Takaya Inamori, Dept. Aerospace Engineering
15:35 - 15:45 Completion ceremony

* We invite the prospective JUACEP participants and engineering students interested in studying abroad to participate and ask any questions related to the program.



Japan-US-Canada Advanced
Collaborative Education program
052-789-2799 JUACEP Office
<https://www.juacep.engg.nagoya-u.ac.jp/>



COMBINATORIAL OPTIMIZATION FOR GEOSPATIAL WIND TURBINE PLACEMENT

Yu-Hsin Wu

Department of Electrical Engineering, Graduate School of Engineering
wu.yu-hsin.t7@s.mail.nagoya-u.ac.jp

Supervisor: Antoine Lesage-Landry

) Department of Electrical Engineering, Polytechnique Montréal
antoine.lesage-landry@polymtl.ca

October 9, 2023

abstract

This study explores combinatorial optimization methods for the strategic placement of wind turbines (WT) based on geospatial data. Leveraging both topographical and meteorological data, the research employs convex optimization to formulate an optimization problem targeted at identifying optimal WT installation sites. The proposed approach assesses multiple placement strategies by taking into account wind patterns, land use restrictions, environmental concerns, and infrastructure limitations, aiming to maximize power generation with minimized power variance and cost. By considering a broader spectrum of factors, this methodology offers a more pragmatic solution compared to conventional methods. Preliminary tests have demonstrated the algorithm's capability to determine optimal WT placements across two basic scenarios. The findings of this research lay the groundwork for an efficient, scalable approach to wind energy projects, positioning the wind energy industry for enhanced feasibility and expansion.

Undisclosed

Pseudocapacitance of T-Nb₂O₅ nanoparticles

Koyo Ueno

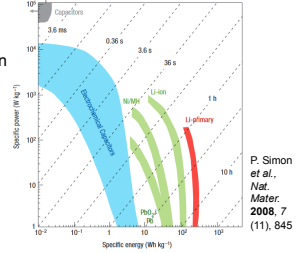
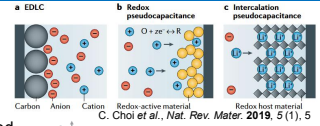


Introduction

2

Pseudocapacitive materials

- Have higher energy density and power density
- Basic mechanisms has been understood (surface redox reaction, fast intercalation)
- There is no ability to predict whether known materials show psuedocapacive behavior and to design a material that exhibits that behavior



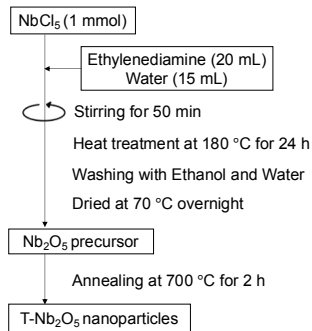
Research Goal

- See what physico-chemical properties (crystalline structures, morphologies, sizes) can control pseudocapacances
- Correct datas on T-Nb₂O₅ nanoparticles

Core set of materials:
Nb₂O₅, MnO₂, MoO₂, TiO₂, TaS₂

T-Nb₂O₅ nanoparticles synthesis via hydrothermal reaction

3



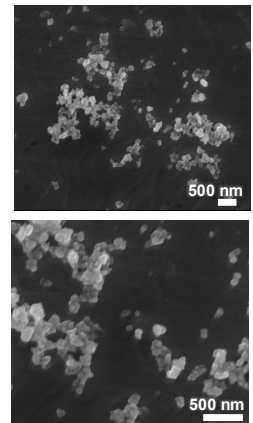
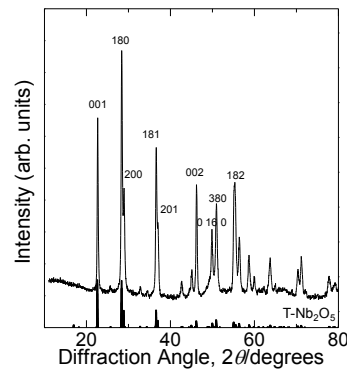
Sample preparation for three electrode cell
T-Nb₂O₅ nps dissolved in ethanol were cast onto stainless steel current collector (~10 μg/cm²)
Heat treatment at 150 °C over night
Dried at 100 °C under vacuum over night
Electrolyte: 1 M LiClO₄ in PC
Counter, Reference electrode: Li metal

Sample preparation for coin cell
T-Nb₂O₅ nps were mixed with carbon black and PVDF in NMP (85:8:7 in weight ratio)
Casted on carbon coated aluminum foil
Dried at r.t. over night
Dried at 70 °C for 6 h
Dried at 100 °C under vacuum over night
Electrolyte: 1 M LiClO₄ in PC
Counter electrode: Li metal

Liao et al., Chinese Chem. Letters, 2018 29, 1785-1790

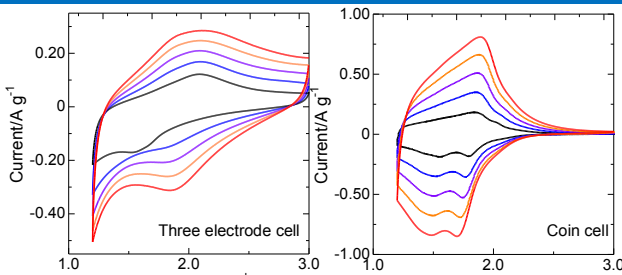
Crystalline Phase and Morphology

4



CV with two different cells

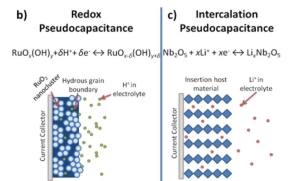
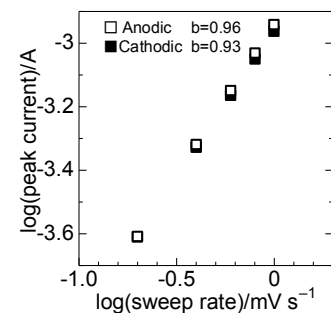
5



Sweep rate/ mV s ⁻¹	Capacity with 3-Electrode Cell/ mAh g ⁻¹	Capacity with Coin Cell/ mAh g ⁻¹
0.2	180	168
0.4	130	164
0.6	111	161
0.8	102	159
1.0	97	157

Kinetics of redox reaction

6

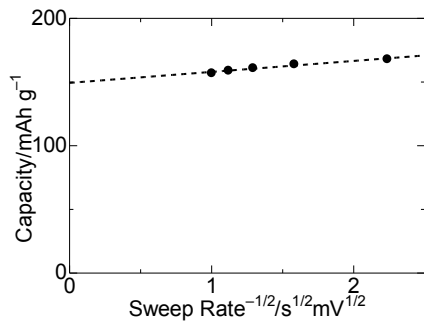


$I = av^b$
I: peak current /A
v: sweep rate /mVs⁻¹
b=0.5: diffusion-controlled (=slow)
b=1 : surface-controlled(=fast)

The redox reaction of T-Nb₂O₅ was surface-controlled

Capacity contribution

7



$$Q(v) = Q_{\text{capacitive}} + Q_{\text{bulk}}$$

(=y-intercept) (=constant($v^{-1/2}$))

The contribution of diffusion process to total amount of charge storage was only 10 % even at slow sweep rate of 0.2 mV s $^{-1}$

Trasatti, S. et al., *Electrochimica Acta* 1990, 35 (1), 263

Conclusion

8

Pseudocapacitance of T-Nb $_2$ O $_5$ <100 nm nanoparticles was investigated.

The redox reaction of T-Nb $_2$ O $_5$ was mainly surface-controlled.

Even at slow sweep rate of 0.2 mV, 90 % of capacity was contributed from capacitive process.

Future work

Further research with faster sweep rate, thicker electrode, and also different materials, morphologies, sizes are essential.

Pseudocapacitance of T-Nb₂O₅ Nanoparticles

Koyo Ueno

Department of Materials Chemistry, Graduate School of Engineering, Nagoya university
ueno.koyo.z0@s.mail.nagoya-u.ac.jp

Supervisor: Professor Bruce Dunn

Department of Materials Science and Engineering, University of California, Los Angeles
bdunn@ucla.edu**ABSTRACT**

Pseudocapacitive materials has recently attracted much attention due to its several attractive properties compared to batteries, such as higher power, faster charging, and a longer cycle life. The mechanism of pseudocapacitance consist fast and reversible surface, or near-surface redox reactions. While underlying features of pseudocapacitance are understood, there is currently no ability to predict or design materials that display pseudocapacitance. This research is a part of a project to discover high-performance pseudocapacitive materials using both of experimental and computational methods. To accomplish this objective, the database of materials including its physico-chemical properties is needed. T-Nb₂O₅ is known as one of the most promising pseudocapacitive materials. In this research, T-Nb₂O₅ nanoparticles were synthesized and their electrochemical properties were investigated.

1. INTRODUCTION

Energy storage devices with high energy density and stable cycling performance are needed to improve for the development of electric vehicles and the power grid.¹ Batteries have high energy density but it takes several hours to recharge. This is because their charge storage mechanism is based on insertion of ions that enables redox reaction in bulk electrode material, that is diffusion controlled and can be slow. However, supercapacitors, or electrical double-layer capacitors (EDLCs), are used for rapid power delivery and fast recharging.² This because their charge storage mechanism is based on adsorption of ions onto the surface of electrode materials. Fig. 1 shows a Ragone plot, that compares their power density and energy density. Pseudocapacitive materials are based on battery-like redox reactions which occur at rates comparable to EDLCs.³ The redox reactions occur at or near-surface of redox-active material. Moreover, intercalation pseudocapacitance occurs when ions intercalate into the channels or layers of redox-active materials by faradaic charge transfer. In Fig. 2, those mechanisms are illustrated. There are two important difference between intercalation pseudocapacitor and battery materials. First, the charge storage mechanism of battery materials is controlled by ion diffusion limitations. However, intercalation pseudocapacitance is not diffusion controlled. Second, materials that exhibit intercalation pseudocapacitance do not undergo phase

transitions therefore increasing kinetics and extending cycle lifetimes. Thus, pseudocapacitor has higher energy density than EDLCs and higher power density than batteries.

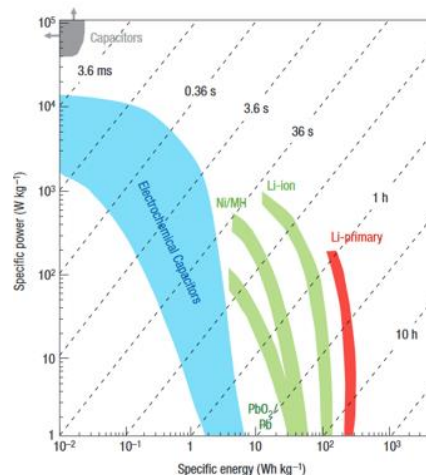


Fig. 1. Specific power against specific energy for various electrical energy storage devices⁴

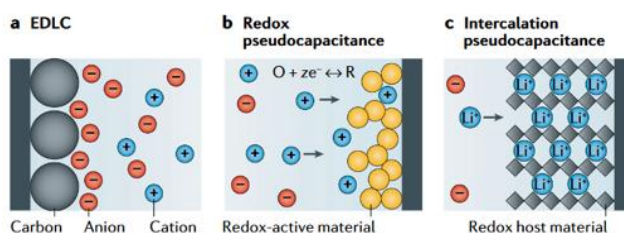


Fig. 2. Electrochemical charge storage mechanisms³

Although fundamental features of pseudocapacitance are understood, currently the ability to predict or design materials that display pseudocapacitance does not exist. This research is a part of a project whose goal is to discover high-performance pseudocapacitive materials using both of experimental and computational methods. To accomplish this objective, the database of materials including its physico-chemical properties is needed. Orthorhombic Nb₂O₅ (T-Nb₂O₅) is found to exhibit fast pseudocapacitive Li⁺ storage.^{5,6} In this research, T-Nb₂O₅ nanoparticles were synthesized and their electrochemical properties were investigated. Other than this work, the database will include MnO₂, anatase TiO₂, TiO₂(B), MoO₂ etc. Also, different sizes and

morphologies and doping of materials will be investigated in this whole project.

2. EXPERIMENTAL METHOD

The synthesis of T-Nb₂O₅ nanoparticles is reported previously.⁷ T-Nb₂O₅ nanoparticles were synthesized by solvothermal method, followed by thermal conversion process. 1 mmol NbCl₅ was dissolved in 20 mL of ethylenediamine and 15 mL of deionized water and stirred for 50 min. This precursor solution was slowly poured into the Teflon-lined autoclave, which kept at 180 °C for 24 hours in oven. After cooling to room temperature naturally, the Nb₂O₅-precursor was centrifuged and rinsed with deionized water and ethanol thoroughly for 3 times and dried at 70 °C for 16 hours. The dried Nb₂O₅ precursor was annealed at 700 °C for 2 hours with a 5 °C min⁻¹ heating rate.

The phase of T-Nb₂O₅ was identified by X-ray diffraction (XRD) using PANalytical X'Pert Pro diffractometer. An X'Celerator detector with Cu Kα1-Kα2 (λ = 1.540598, 1.54426 Å) radiation was used.

The morphology and particle size were characterized by Scanning electron microscopy (SEM; FEI Nova NanoSEM230) with an accelerating voltage of 7 kV. SEM samples were prepared as the same way of preparing thin electrode with suspension and stainless-steel foil (mentioned later.)

Electrochemical measurements were performed in a three-electrode cell and in a 2032 type coin cell. The thin electrode for three-electrode cell was fabricated by drop-casting a well-sonicated suspension of T-Nb₂O₅ (≈10 μg) in ethanol on an oxygen plasma treated stainless-steel foil (≈1 cm² area) (Alfa Aesar). The mass of the nanoparticles deposited on the stainless-steel foil was determined using a microbalance. For measurements in three-electrode cell, lithium foils (Sigma-Aldrich) served as the reference and counter electrodes, and the electrolyte was 1 M LiClO₄ (Sigma-Aldrich) in propylene carbonate (Sigma-Aldrich). The thick electrode for the coin cell was prepared by mixing the active material, carbon black (Timcal Super C65) and PVdF (Kynar) binder in 85:8:7 weight ratio. The slurry was drop-cast onto 10-mm-diameter carbon coated aluminum disc current collectors and dried at 70 °C for 16 hours and at 100 °C under vacuum for 6 hours. The electrode loading was between 1 and 1.5 mg cm⁻². For measurements in coin cell, lithium foil was used as anode with the glass fiber separator (Whatman, GF/A) saturated with 1 M LiClO₄ in propylene carbonate. All cells were assembled in argon filled glove box with the H₂O and O₂ level below 0.1 ppm and measurements for three-electrodes were performed in the glove box.

Electrochemical measurements were performed between 1.2 and 3 V vs. Li/Li⁺ using a PAR EG&G 273A Potentiostat.

3. RESULTS AND DISCUSSION

The XRD pattern of synthesized Nb₂O₅ sample is shown in Fig. 3. The diffraction peaks belonged to an

orthorhombic phase. (JCPDS-30-0873, a = 6.175 Å, b = 29.175 Å, c = 3.930 Å; space group: Pbam(55))

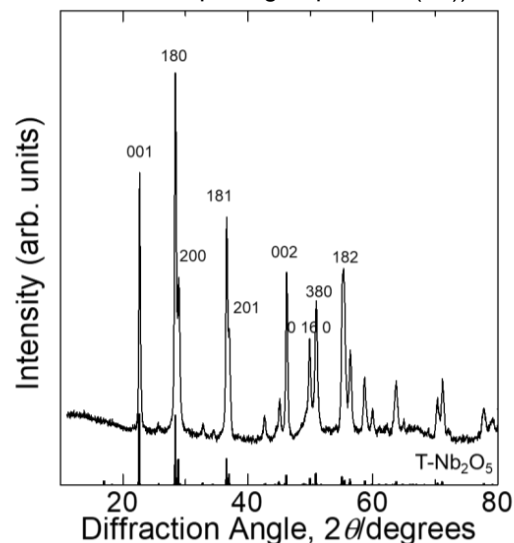


Fig. 3 XRD pattern of synthesized T-Nb₂O₅

The morphology of T-Nb₂O₅ was characterized with SEM. As shown in Fig 4, nanoparticles were obtained and their particle size was ~100 nm. Some of the particles still agglomerated even though the suspension was sonicated. The method to solve this agglomeration problem should be optimized further to improve its electrochemical properties.

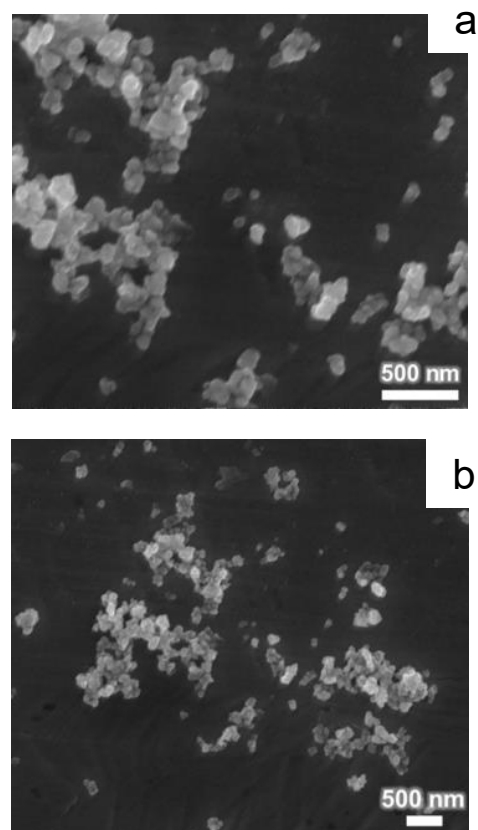
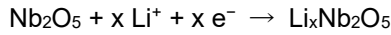


Fig. 4 (a,b) morphologies of T-Nb₂O₅ nanoparticles on stainless steel foil

2-2. 2023 Medium-term course at UCLA and NCSU

Cyclic voltammetry (CV) was used to determine the electrochemical properties of the T-Nb₂O₅ nanoparticles. The sweep rate were varied from 0.2-1.0 mV s⁻¹ between 1.2-3.0 V vs.Li/Li⁺. For Nb₂O₅ in a lithium ion cell, charge storage occurs through the insertion of lithium ions with concomitant reduction of Nb⁵⁺ to Nb⁴⁺, for a maximum theoretical storage of x=2 and theoretical capacity is 202 mAhg⁻¹:⁸



The working electrode of three electrode cell had only T-Nb₂O₅ active material, which means there should be a problem about its electron conduction from the current collector to active material and also about detaching of the material. In coin cell, the working electrode contained conductive carbon and binder. These differences could have affected the results of electrochemical tests.

Fig. 5 and 6 are CVs with three electrode cell and coin cell respectively. The value of peak current and its broadness were different between two different setups. In Fig5, broad cathodic and anodic peaks can be seen around 2.1 V and 1.8 V. In Fig 6, cathodic peak can be seen around 1.9 V and two anodic peaks can be seen around 1.4 and 1.7 V. Capacity dependence on sweep rate with two different setups are shown in Table1. At higher sweep rate, higher capacity was achieved with coin cell. This could be due to the difference of electron conduction between two setups.

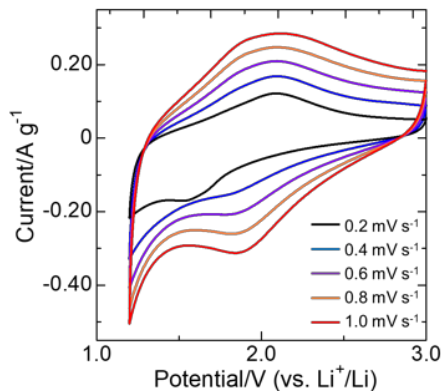


Fig. 5. CV with three electrode cell

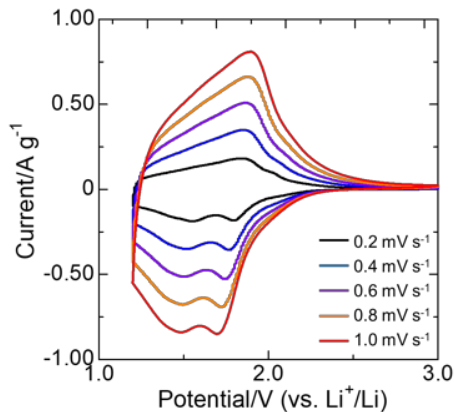


Fig. 6. CV with coin cell

Sweep rate/ mV s ⁻¹	Capacity with 3-Electrode Cell / mAh g ⁻¹	Capacity with Coin Cell / mAh g ⁻¹
0.2	180	168
0.4	130	164
0.6	111	161
0.8	102	159
1.0	97	157

To characterize kinetics, we take advantage of being able to generalize the peak current (*i*) variation with sweep rate (*v*) as: $i = av^b$, where *a* and *b* are adjustable values.⁹ Whereas a *b*-value of 0.5 would indicate that the current is controlled by semi-infinite linear diffusion, a value of 1 indicates that the current is surface-controlled. In the CV with three electrode cell (Fig 5), the peaks are so broad that the *b*-value may not be useful to characterize the kinetics. However, the CV with coin cell (Fig 6) has sharper peaks to get *b*-value. As in Fig 8, the *b*-value with coin cell is close to 1. In this sweep rate range, it can be said the current was surface-controlled.

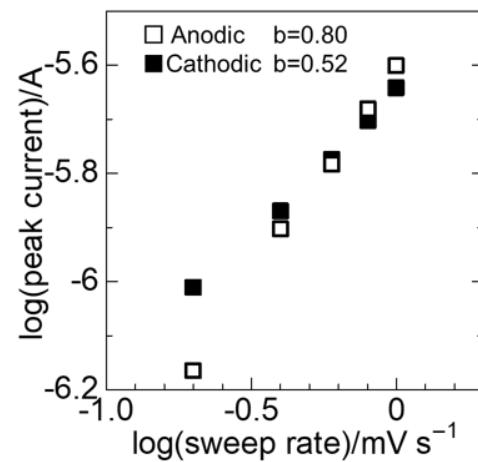


Fig. 7. Peak current dependence on sweep rate with three electrode cell

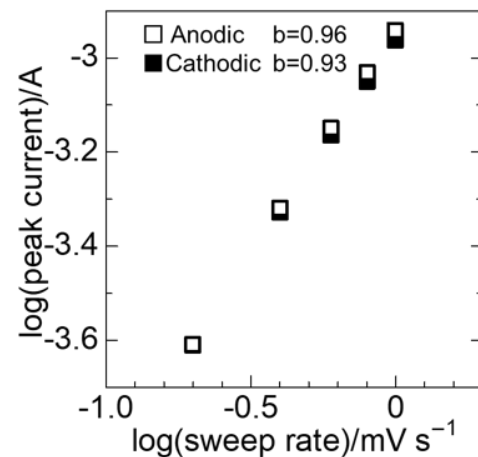


Fig. 8. Peak current dependence on sweep rate with coin cell

To obtain further insight concerning the kinetics of charge storage in T-Nb₂O₅, we adapted an analysis first used by Trasatti et al. to characterize the charge storage of RuO₂, a well known pseudocapacitive material.¹⁰ In this analysis, the overall capacity (Q) of a material is assumed to contain two contributions, that from capacitive charge storage ($Q_{capacitive}$, the “outer surface”) and that from bulk charge storage (Q_{bulk} , the “inner surface”):

$$Q = Q_{capacitive} + Q_{bulk} \quad (1)$$

The bulk charge storage depends upon ion diffusion and, assuming semi-infinite linear diffusion, is expected to vary as $t^{1/2}$. By rewriting the above equation in terms of the sweep rate (v), the following relationship arises:

$$Q(v) = Q_{capacitive} + constant(v^{-1/2}) \quad (2)$$

In this analysis, a plot of capacity vs. $v^{-1/2}$ yields a straight line whose y-intercept ($v=\infty$) is the “outer surface” capacity or the infinite-sweep rate capacity. Due to the possibility of polarization at high sweep rates, deviation from a straight line usually occurs, and intermediate sweep rates are then selected to extrapolate to the y-intercept.^{5,11}

As in Fig.10, the capacity of infinite sweep rate was $\sim 150 \text{ mAh g}^{-1}$. At the sweep rate of 0.2 and 1.0 mV s^{-1} , the contribution of diffusion process to total amount of charge storage was only 10 and 5%, respectively.

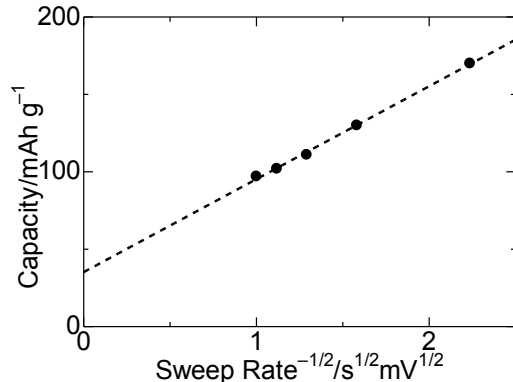


Fig. 9. The capacity as a function of sweep rate^{1/2} with three electrode cell

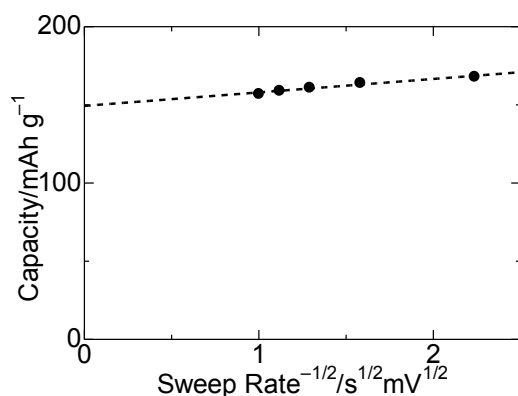


Fig. 10. The capacity as a function of sweep rate^{1/2} with coin cell

4. CONCLUSION

In this research, pseudocapacitance of T-Nb₂O₅ nanoparticles is investigated following previous reports.⁵⁻⁷ The result was consistent with them. This research will be a part of establishing a system to discover high-performance pseudocapacitive materials. Further research on different particle sizes, morphologies, sorts of materials is needed for further progress of this project.

ACKNOWLEDGEMENTS

I would like to thank Professor Bruce Dunn for giving me a great opportunity to do research in UCLA. I also really appreciate that Dr. Andrea Zambotti, a post doctor in Dunn's group helped me a lot in on this research. I also would like to thank JUACEP for supporting my stay at UCLA. Finally, I would like to thank my supervisors, Kazuki Nakanishi and George Hasegawa for allowing me to join this program.

REFERENCES

- (1) Conway, B. E.; Pell, W. G. Double-Layer and Pseudocapacitance Types of Electrochemical Capacitors and Their Applications to the Development of Hybrid Devices. *J. Solid State Electrochem.* **2003**, *7* (9), 637–644. <https://doi.org/10.1007/s10008-003-0395-7>.
- (2) Simon, P.; Gogotsi, Y.; Dunn, B. Where Do Batteries End and Supercapacitors Begin? *Science* **2014**, *343* (6176), 1210–1211. <https://doi.org/10.1126/science.1249625>.
- (3) Choi, C.; Ashby, D. S.; Butts, D. M.; DeBlock, R. H.; Wei, Q.; Lau, J.; Dunn, B. Achieving High Energy Density and High Power Density with Pseudocapacitive Materials. *Nat. Rev. Mater.* **2019**, *5* (1), 5–19. <https://doi.org/10.1038/s41578-019-0142-z>.
- (4) Simon, P.; Gogotsi, Y. Materials for Electrochemical Capacitors. *Nat. Mater.* **2008**, *7* (11), 845–854. <https://doi.org/10.1038/nmat2297>.
- (5) Kim, J. W.; Augustyn, V.; Dunn, B. The Effect of Crystallinity on the Rapid Pseudocapacitive Response of Nb₂O₅. *Adv. Energy Mater.* **2012**, *2* (1), 141–148. <https://doi.org/10.1002/aenm.201100494>.
- (6) Augustyn, V.; Come, J.; Lowe, M. A.; Kim, J. W.; Taberna, P.-L.; Tolbert, S. H.; Abruña, H. D.; Simon, P.; Dunn, B. High-Rate Electrochemical Energy Storage through Li⁺ Intercalation Pseudocapacitance. *Nat. Mater.* **2013**, *12* (6), 518–522. <https://doi.org/10.1038/nmat3601>.
- (7) Liao, J.; Tan, R.; Kuang, Z.; Cui, C.; Wei, Z.; Deng, X.; Yan, Z.; Feng, Y.; Li, F.; Wang, C.; Ma, J. Controlling the Morphology, Size and Phase of Nb₂O₅ Crystals for High Electrochemical Performance. *Chin. Chem. Lett.* **2018**, *29* (12), 1785–1790. <https://doi.org/10.1016/j.ccllet.2018.11.018>.

2-2. 2023 Medium-term course at UCLA and NCSU

JUACEP Independent Research Report
Nagoya University, Japan

(8) Ohzuku, T.; Sawai, K. ELECTROCHEMISTRY OF L-NIOBIUM PENTOXIDE IN A LITHIUM/NON-AQUEOUS CELL.

(9) Lindström, H.; Södergren, S.; Solbrand, A.; Rensmo, H.; Hjelm, J.; Hagfeldt, A.; Lindquist, S.-E. Li⁺ Ion Insertion in TiO₂ (Anatase). 2. Voltammetry on Nanoporous Films. *J. Phys. Chem. B* **1997**, *101* (39), 7717–7722. <https://doi.org/10.1021/jp970490q>.

(10) Ardizzone, S.; Fregonara, G.; Trasatti, S. “Inner” and “Outer” Active Surface of RuO₂ Electrodes. *Electrochimica Acta* **1990**, *35* (1), 263–267. [https://doi.org/10.1016/0013-4686\(90\)85068-X](https://doi.org/10.1016/0013-4686(90)85068-X).

(11) Baronetto, D.; Krstajić, N.; Trasatti, S. Reply to “Note on a Method to Interrelate Inner and Outer Electrode Areas” by H. Vogt. *Electrochimica Acta* **1994**, *39* (16), 2359–2362. [https://doi.org/10.1016/0013-4686\(94\)E0158-K](https://doi.org/10.1016/0013-4686(94)E0158-K).

Investigation of Ionic conductivity of Ionogel Electrolyte on separator

Koyo Ueno



Introduction

10

Ionogel Electrolyte

Immobilizing ionic liquid while keeping its unique properties

- ✓ Negligible vapor pressure
- ✓ Thermal stability
- ✓ Non-flammability
- ✓ Wide electrochemical stability window
- ✓ High ionic conductivity



Research Goal

To fabricate ionogel on separator that has high ionic conductivity
 Advantage: separator provides structural support for thin ionogel → easy to handle in setting up battery cells

Synthesis method

11

Compound	Ratio(vol)
MTMS	1.5
TMOS	2
Formic acid	2
0.5 M LiFSI in PYR13FSI	6,8,12,16

TMOS, MTMS, Formic acid
 → Stirring at r.t. for 1 h
 → 0.5 M LiFSI in PYR13FSI
 → Mixing with vortex for 10 s
 → Casting to mold
 → Drying at r.t. for 24 h → Monolith ionogel
 → Drying at 70 °C for 5 h
 → Dip Φ16mm Separator → Drying at r.t. for 24 h → Ionogel on Separator
 → Drying at 70 °C for 5 h

[Li+].[F-]S(=O)(=O)N(S(=O)(=O)F)S(=O)(=O)F
 LIFSI

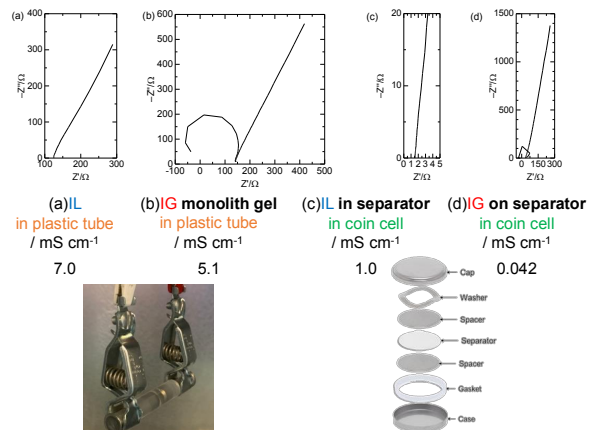
CC[N+](C)(C)C(F)(F)O2.[F-]S(=O)(=O)N(S(=O)(=O)F)S(=O)(=O)F
 PYR13FSI

CC[N+](C)(C)C(F)(F)O2
 (FSO₂)₂N⁻

P. McNeil UCLA doctoral thesis 2023

Conductivities of each samples

12

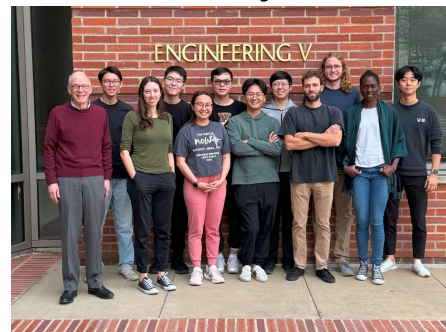


Conclusion

13

- Monolith ionogel and thin ionogel on the separator were fabricated by sol-gel process.
- The conductivity of the thin ionogel on separator was much lower compared to that of ionic liquid in separator, whereas the conductivity of the monolith gel was similar to the neat ionic liquid.

Thank you!



Investigation of Ionic conductivity of Ionogel Electrolyte on separator

Koyo Ueno

Department of Materials Chemistry, Graduate School of Engineering, Nagoya University
ueno.koyo.z0@s.mail.nagoya-u.ac.jp

Supervisor: Professor Bruce Dunn

Department of Materials Science and Engineering, University of California, Los Angeles
bdunn@ucla.edu

ABSTRACT

Ionogels have recently attracted attention as pseudo-solid-state electrolytes based on their ability to confine Ionic Liquids (ILs) within the mesoporous network of a sol-gel-derived inorganic matrix. ILs have some unique properties, such as negligible vapor pressure, thermal stability, and non-flammability, combined with high ionic conductivity and wide electrochemical stability window.

In this work, the thin ionogel was fabricated on the separator for practical application. Separator working as a substrate will give ionogel mechanical strength and make it easier to utilize in the commercial batteries. The ionogel on separator is expected to suppress lithium dendrite growth and improve the cycle stability while keeping its high ionic conductivity.

The conductivity of monolith ionogel was $\sim 5 \text{ mS cm}^{-1}$, which was similar to that of neat ionic liquid, that is $\sim 7 \text{ mS cm}^{-1}$. However, the conductivity of thin ionogel on separator was $\sim 0.04 \text{ mS cm}^{-1}$, which was much lower than that of separator saturated with ionic liquid, that is $\sim 1 \text{ mS cm}^{-1}$.

1. INTRODUCTION

Lithium-ion battery is widely used in current society. Organic liquid electrolytes have been used for many years because of its high conductivity and excellent wetting of electrode surfaces. However, those electrolytes have drawbacks that include low thermal and electrochemical stability and relatively low flash points that can lead to flammability risks.¹

Ionogels have received considerable attention because of their unique advantages. Ionogels have silica-based three-dimensional network through which ionic liquid (IL) percolates. ILs consist of organic salts which have low melting point below $100 \text{ }^\circ\text{C}$. ILs have been expected to be a replacement for traditional organic electrolytes due to their negligible vapor pressure, thermal stability and non-flammability, combined with high ionic conductivity and wide electrochemical stability window. Ionogel is one of the ways to immobilize the ILs. Normally gel is made by allowing the liquid phase to evaporate and leave behind the porous gel. Because ILs have negligible vapor pressure, they are able to remain inside the gel network.

2-5

In this work, the separator was employed to provide structural support for thin ionogel by working as a separator, thereby enhancing its stability and functionality within the experimental setup. The object of this research is to fabricate thin ionogel on the separator that has high ionic conductivity and improves cycle stability.

2. EXPERIMENTAL METHOD

The ionogels were made by a standard sol-gel process. The synthesis of the ionogel is reported previously.⁶ A solution containing Methyltrimethoxysilane (MTMS), Tetramethyl orthosilicate (TMOS), Formic Acid mixed in a ratio of 1:1.28:5.04 mols (1.5:2:2 in volume) of MTMS: TMOS: Formic Acid. The sol was allowed to mix for 1 hour before adding the ionic liquid. The ionic liquid was prepared by dissolving 0.5 mmol of LiFSI per 1 mL of PYR13FSI and stored in argon-filled glove box. The amount of ionic liquid was varied from 8, 12, and 16 in a volumetric ratio to 1.5 of MTMS, 2 of TMOS, 2 of Formic Acid.

After the ionic liquid was added, the solution was mixed for 30 seconds and casted into plastic cap. Separator (Celgard 2500) was dipped in ethanol briefly and then soaked in the casted solution under vacuum for 10 minutes. After 10 minutes, the celgard separators containing casted solution were put on Teflon sheet and dried for ~ 18 hours at room temperature and at $70 \text{ }^\circ\text{C}$ for 6 hours. This is the fabrication process of thin ionogel on separator. The thickness of thin ionogel on separator was $\sim 30 \text{ }\mu\text{m}$ including Celgard 2500, whose thickness is $25 \text{ }\mu\text{m}$. The rest solution in the plastic cap was dried in the same way and the monolith ionogel was obtained.

The monolith ionogels were placed between stainless steel stubs in plastic tube to perform electrochemical measurements as in figure 1. Electrochemical measurements on gels on the separator were performed in coin cells. The separators with thin ionogel were placed between two stainless steel spacers in a coin cell. For reference, ionic liquid was placed between stainless steel stubs in plastic tube. Also, separators saturated with ionic liquid were tested in a coin cell. Ionic conductivities for both ionic liquid and ionogels were calculated from electrochemical impedance spectroscopy (EIS). An AC voltage of 10 mV was applied with frequencies ranging from 100 Hz to 1 MHz.

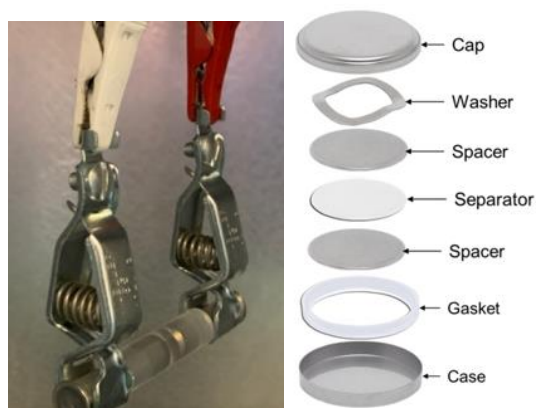


Fig 1. (left) plastic tube setup (right) coin cell setup for electrochemical measurements

3. RESULTS AND DISCUSSION

Monolith ionogel and ionogel on separator were transparent and homogenized as in Fig 2.



Fig2. Appearance of monolith ionogel (left) and thin ionogel on separator (right)

The results of EIS were shown in Fig3(a)-(d). The resistance of each sample was calculated from the intersection of x-axis and the spike line. The resistance was converted to conductivities with Eq.1. The ionic conductivity of each sample was shown in Table 1. Monolith ionogel had similar conductivity with neat ionic liquid. The conductivity of ionic liquid in separator was lower than neat ionic liquid. However, this result is consistent with other reports.⁷ Considering the porosity of Celgard 2500 is 55%, this value could be reasonable.

While the monolith ionogel retained good conductivity compared to neat ionic liquid, ionogel on separator showed much lower conductivity compared to ionic liquid in separator. As in Table 2, the amount of ionic liquid in the ionogel had little influence on its conductivity. It can be said that the amount of ionic liquid is not a cause of the poor ionic conductivity. The low conductivity could be because the pathway of the ionic liquid was narrow in the separator and gel matrix.

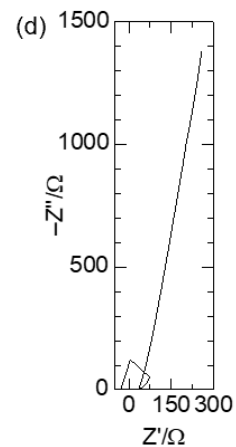
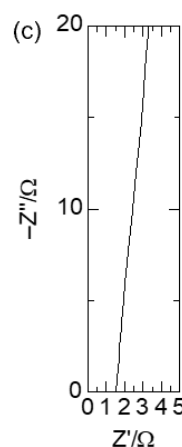
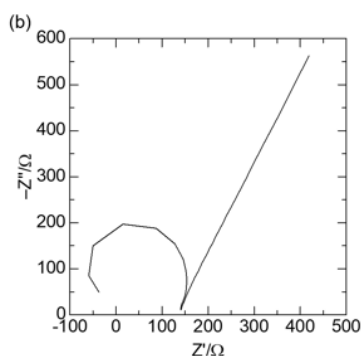
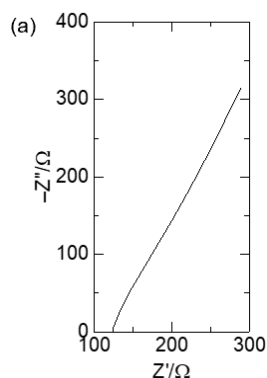


Fig3. Nyquist plot examples of (a) ionic liquid, (b) Monolith ionogel, (c) ionic liquid in separator, (d) Thin ionogel on separator

$$\sigma = \frac{L}{R \times A} \text{ (Eq.1)}$$

σ : conductivity (S cm⁻¹)
L: thickness of the sample (cm)
A: Area of the sample (cm²)
R: measured resistance (Ω)

Table1. Ionic conductivities of each sample

Samples	Ionic conductivity (mS cm ⁻¹)
ionic liquid	7.0
Monolith ionogel	5.1
ionic liquid in separator	1.0
Ionogel on separator	0.042

Table 2. Conductivities of ionogel samples with different amount of ionic liquid

Amount of ionic liquid	800	1200	1600
Conductivity of monolith ionogel / mS cm ⁻¹	5.1	4.7	6.3
Conductivity of ionogel on separator / mS cm ⁻¹	0.042	0.033	0.042

4. CONCLUSION

In this research the monolith ionogel and thin ionogel on the separator were fabricated by sol-gel process. Their conductivities were measured by EIS in the plastic tube or in the coin cell. The conductivity of the monolith gel was similar to the neat ionic liquid. However, the conductivity of thin ionogel on separator was much lower compared to that of ionic liquid in separator. This could be because the pathway of the ionic liquid was too narrow in the gel matrix in the separator.

ACKNOWLEDGEMENTS

I would like to thank Professor Bruce Dunn for giving me a great opportunity to do research in UCLA. This research is also supported by Dr. Ryo Tamaki in Paradigm energy. I also would like to thank JUACEP for supporting my stay at UCLA. Finally, I would like to thank my supervisors, Kazuki Nakanishi and George Hasegawa for allowing me to join this program.

REFERENCES

- (1) Manthiram, A.; Yu, X.; Wang, S. Lithium Battery Chemistries Enabled by Solid-State Electrolytes. *Nat. Rev. Mater.* **2017**, *2* (4), 1–16. <https://doi.org/10.1038/natrevmats.2016.103>.
- (2) Ashby, D. S.; DeBlock, R. H.; Lai, C.-H.; Choi, C. S.; Dunn, B. S. Patternable, Solution-Processed Ionogels for Thin-Film Lithium-Ion Electrolytes. *Joule* **2017**, *1* (2), 344–358. <https://doi.org/10.1016/j.joule.2017.08.012>.
- (3) Le Bideau, J.; Viau, L.; Vioux, A. Ionogels, Ionic Liquid Based Hybrid Materials. *Chem Soc Rev* **2011**, *40* (2), 907–925. <https://doi.org/10.1039/C0CS00059K>.
- (4) Fan, X.; Liu, S.; Jia, Z.; Koh, J. J.; Yeo, J. C. C.; Wang, C.-G.; Suratman, N. E.; Loh, X. J.; Bideau, J. L.; He, C.; Li, Z.; Loh, T.-P. Ionogels: Recent Advances in Design, Material Properties and Emerging Biomedical Applications. *Chem. Soc. Rev.* **2023**, *52* (7), 2497–2527. <https://doi.org/10.1039/D2CS00652A>.
- (5) DeBlock, R. H.; Wei, Q.; Ashby, D. S.; Butts, D. M.; Whang, G. J.; Choi, C. S.; Dunn, B. S. Siloxane-Modified, Silica-Based Ionogel as a Pseudosolid Electrolyte for Sodium-Ion

Batteries. *ACS Appl. Energy Mater.* **2021**, *4* (1), 154–163.

<https://doi.org/10.1021/acsaem.0c02055>.

- (6) McNeil, P. E. Transport Properties and Performance in Amorphous Silica and Amorphous Metal Oxide Materials. **2023**.

- (7) Kirchhöfer, M.; Von Zamory, J.; Paillard, E.; Passerini, S. Separators for Li-Ion and Li-Metal Battery Including Ionic Liquid Based Electrolytes Based on the TFSI⁻ and FSI⁻ Anions. *Int. J. Mol. Sci.* **2014**, *15* (8), 14868–14890. <https://doi.org/10.3390/ijms150814868>.

NC STATE UNIVERSITY

名古屋大学
NAGOYA UNIVERSITY

On the frequency lock-on within a network of oscillators using phase-reduction analysis

Kaito Usami
 NCSU, Department of Mechanical and Aerospace engineering
 Supervisor : Prof. Chi-An Yeh
 NU Department of Aerospace engineering, Supervisor : Prof. Takaya Inamori
 April 18, 2024

1

NC STATE UNIVERSITY

名古屋大学
NAGOYA UNIVERSITY

Today Outline

1. Background of limit-cycle oscillator
 - Conventional method to reveal the requirements their features
 - Problem of the methods and Purpose of my research
2. Consideration 1 to reveal the global-coupling conditions
 - Result 1 for global coupling
 - Consideration 2 to reveal the Lock-on conditions on multiple oscillators
 - Result 2 for lock on
3. Conclusions
 - Combining with research in NU

2

NC STATE UNIVERSITY

名古屋大学
NAGOYA UNIVERSITY

Backgrounds

Rhythmic nonlinear dynamical systems in our world

- Flashing fireflies^[1]
- Mechanical vibrations^[2]
- Pendulum clock^[3]

→ “Limit cycle oscillator”

$$\frac{d}{dt} X = F(X) \quad (1)$$

$$X(t) = X(t + 1/f_n) \quad (2)$$

Characteristics of the oscillator's frequency f_n

1. Lock-on by external periodic force

$f_n \neq f_{ext} \rightarrow f_n = f_{ext}$

[Fig.1] Controlling frequency of shedding by bottom actuators^[4]

2. Global coupling by internal network

$f_{n1} \neq f_{n2} \neq \dots \neq f_{nN} \rightarrow f_{n1} = f_{n2} = \dots = f_{nN}$

[Fig.2] Synchronization of flashing fireflies^[5]

This physics is high dimensional to reveal the condition to perform these features.

3

NC STATE UNIVERSITY

名古屋大学
NAGOYA UNIVERSITY

Conventional method to reveal Lock-on's requirements

Phase-reduction analysis^[6]

- The complex dynamics are described by only a single "phase" variable within the condition the external perturbations are sufficiently weak.

$$\frac{d}{dt} X = F(X) + \epsilon \sin(2\pi f_{ext} t) \quad (1)$$

The "phase function" that their state translate to phase on the limit cycle χ is defined by

$$\theta(X(t)) \equiv \theta(t) \quad (2)$$

When this oscillator is perturbed by a small vector I , "phase function" can be expanded in a Taylor series

$$\theta(X(t) + I) = \theta(X(t)) + \nabla \theta(X) \Big|_{X=\chi} \cdot I + O(|I|^2) \quad (3)$$

This part must determine the influence of the perturbation function.
In this method, they call it "phase-sensitivity function" with $Z(\theta)$.

Impulse at θ Phase difference $\Delta\theta = Z(\theta) \cdot I$

4

NC STATE UNIVERSITY

名古屋大学
NAGOYA UNIVERSITY

Conventional method to reveal Lock-on's requirements

The relative phase variable is defined as follow

$$\phi(t) = \theta(X(t)) - 2\pi f_{ext} t \quad (1)$$

where f_{ext} is the frequency of the external forcing.

The "phase coupling function" is defined with

$$\Gamma(\phi) = \frac{1}{2\pi} \int_0^{2\pi} Z(\phi + \psi) \cdot f \left(\frac{\psi}{\Omega} \right) d\psi \quad (2)$$

The function $\Gamma(\phi)$ indicate how huge difference is happen by external perturbation for one period of external forcing.

Under this approximation, the phase function is written in

$$\frac{d}{dt} \phi(t) = 2\pi f_n - 2\pi f_{ext} + \epsilon \Gamma(\phi) \quad (3)$$

If this function satisfies the inequality

$$\frac{\epsilon}{2\pi} \min_{\psi} \Gamma(\phi) < f_n - f_{ext} < \frac{\epsilon}{2\pi} \max_{\psi} \Gamma(\phi) \quad (4)$$

whether these oscillators are Lock-on or not Lock-on can be estimated.

5

NC STATE UNIVERSITY

名古屋大学
NAGOYA UNIVERSITY

Lock-on criteria in the Single oscillator External force

The Criteria By full nonlinear simulation vs. By phase-reduction analysis in the single oscillator

[Fig.3] Full nonlinear simulation

[Fig.4] Estimation by phase-reduction analysis

- The external force which has more powerful or close frequency can make the oscillator Lock-on.
- In Fig.4 there is similar relationships between amplitude and frequency.

[Problem] This analysis can not reveal the condition in the multiple oscillators.

[Purpose] Expand it from a single oscillator to multiple oscillators to reveal the condition.

6

NC STATE UNIVERSITY

名古屋大学
NAGOYA UNIVERSITY

Considerations

[Purpose] Expand it from a single oscillator to multiple oscillators to reveal the condition.

[1] Global coupling by internal Gaussian network Multiple

The M -dimensional nonlinear dynamics are written with

$$\frac{d}{dt} X_i(t) = F_i(X_i) + \sum_{j=1}^N A_{ij}(X_i, X_j) \quad (1)$$

where X_i is the i th M -dimensional matrix to represent dynamics state and has a stable limit cycle and $A_{ij}(X_i, X_j)$ is interactive functions between each oscillators according to Gaussian.

[2] Lock-on by external forcing to global-coupling oscillators Multiple

The M -dimensional nonlinear dynamics are written with External force

$$\frac{d}{dt} X_i(t) = F_i(X_i) + \sum_{j=1}^N A_{ij}(X_i, X_j) + \epsilon \sin(\Omega t) \quad (2)$$

where X_i is the i th M -dimensional matrix to represent dynamics state and has a stable limit cycle

NC STATE UNIVERSITY

名古屋大学
NAGOYA UNIVERSITY

Considerations 1 to reveal Global-coupling conditions Multiple

Expansion method 1

Single oscillator

$$\Gamma_i(\varphi) = \frac{1}{2\pi} \int_0^{2\pi} Z_i(\psi + \varphi) \cdot f\left(\frac{\psi}{\Omega}\right) d\psi \quad (1)$$

$\Gamma_i(\varphi)$ shows the effect of external force by inner product of sensitivity function.

Multiple oscillators

$$\Gamma_{ij}(\varphi) = \frac{1}{2\pi} \int_0^{2\pi} Z_i(\psi + \varphi) \cdot A_{ij}(\psi + \varphi, \psi) d\psi \quad (2)$$

$\Gamma_{ij}(\varphi)$ shows the effect of internal network between i and j by inner product of sensitivity function.

Under this approximation, each "phase-coupling function" is overlapped with

$$\frac{d}{dt} \phi_i(t) = \omega_i - \Omega_i + \sum_{j=1}^N \Gamma_{ij}(\phi_i - \phi_j) \quad (3)$$

If this function satisfies the inequality ($i = 1, \dots, N$)

$$\min_{\phi_i} \sum_{j=1}^N \Gamma_{ij}(\phi_i - \phi_j) < \omega_i - \Omega_i < \max_{\phi_i} \sum_{j=1}^N \Gamma_{ij}(\phi_i - \phi_j) \quad (4)$$

Whether these oscillators are global coupling or not it can be estimated.

NC STATE UNIVERSITY

名古屋大学
NAGOYA UNIVERSITY

Result 1 to reveal Global-coupling conditions Multiple

The Criteria By full nonlinear simulation vs. By expanded phase-reduction analysis

[Fig.5] Full nonlinear simulation

[Fig.6] Estimation by "phase coupling function"

- The oscillators with big interaction force are global coupling more easily than one with small.
- The wider Gaussian lets the oscillators coupling easily.
- In Fig.6 similar relationships between interactive function and frequency is existed.

NC STATE UNIVERSITY

名古屋大学
NAGOYA UNIVERSITY

Considerations 2 to reveal Lock-on conditions External force

Expansion method 2

Single oscillator

$$Z(\theta) = \lim_{T \rightarrow \infty} \frac{g(\theta; I\epsilon)}{T} \quad (1)$$

$Z(\theta)$ shows the phase difference of oscillator when the oscillator is kicked sufficiently small.

Multiple oscillators

$Z_{ij}(\theta)$ shows the phase difference of the i th oscillator when the j th oscillator is kicked sufficiently small.

$$\begin{bmatrix} Z_{11}(\theta_1) & \dots & Z_{1N}(\theta_N) \\ \vdots & \ddots & \vdots \\ Z_{N1}(\theta_1) & \dots & Z_{NN}(\theta_N) \end{bmatrix} = \begin{bmatrix} \lim_{T \rightarrow \infty} \frac{g_1(\theta_1; I\epsilon_1)}{T} & \dots & \lim_{T \rightarrow \infty} \frac{g_1(\theta_N; I\epsilon_N)}{T} \\ \vdots & \ddots & \vdots \\ \lim_{T \rightarrow \infty} \frac{g_N(\theta_1; I\epsilon_1)}{T} & \dots & \lim_{T \rightarrow \infty} \frac{g_N(\theta_N; I\epsilon_N)}{T} \end{bmatrix} \quad (2)$$

Under this approximation, "phase coupling function" is determined with

$$\Gamma_{ij}(\varphi) = \frac{1}{2\pi} \int_0^{2\pi} Z_{ij}(\psi + \varphi) \cdot f\left(\frac{\psi}{\Omega}\right) d\psi \quad (3)$$

$$\min_{\phi_i} \sum_{j=1}^N \Gamma_{ij}(\phi_i - \phi_j) < \omega_i - \Omega_i < \max_{\phi_i} \sum_{j=1}^N \Gamma_{ij}(\phi_i - \phi_j) \quad (4)$$

Whether these oscillators are Lock-on or not Lock-on can be estimated.

NC STATE UNIVERSITY

名古屋大学
NAGOYA UNIVERSITY

Result 2 to reveal Lock-on conditions External force

The Criteria By full nonlinear simulation vs. By expanded phase-reduction analysis

[Fig.7] Full nonlinear simulation

[Fig.8] Estimation by "phase coupling function"

- The case that external force is applied in intermediate oscillators is Lock-on easily.
- In Fig.8 there is similar relationships between the forced oscillator and required amplitude.
- In Fig.8 there is the area which has high standard deviation in the case of applying to 3rd oscillator, because it is hard to consider global-coupling network to be linear.

NC STATE UNIVERSITY

名古屋大学
NAGOYA UNIVERSITY

Conclusion

- We propose the expanding way of "phase-reduction analysis" from one oscillator to multiple oscillators.
- In terms of Global coupling, we can estimate the requirements by expanding "phase coupling function".
- In terms of Lock-on on multiple oscillators, we can't capture detailed features.
- From these results, we consider it is hard to consider global-coupling network to be linear.

On the frequency lock-on within a network of oscillators using phase-reduction analysis

Kaito Usami

Department of Aerospace Engineering, Graduate School of Engineering, Nagoya University
usami.kaito.b9@s.mail.nagoya-u.ac.jp

Supervisor: Chi-An Yeh

Department of Mechanical and Aerospace Engineering, North Carolina State University
cyeh4@ncsu.edu

Abstract

There are rhythmic nonlinear dynamical systems in our world known as limit-cycle oscillators. We apply phase-reduction analysis to examine global coupling to multiple oscillators through interactive forces and their synchronization properties to periodic external forces. This analysis allows us to reduce the 3-dimensional dynamics to a single scalar phase variable. We characterize the phase response to impulse perturbations, using this sensitivity function to reveal the conditions for synchronization. The conditions derived from the approximation function closely agree with results from numerical simulations conducted one by one, uncovering global coupling or Lock-on characteristics.

1. Introduction

We can find examples of rhythmic nonlinear dynamical systems in our world, such as the motion of a pendulum clock, flashing fireflies, mechanical vibrations, and vortex shedding after a circular cylinder [1-5]. In this report, we employ a theoretical method for analysing limit-cycle oscillators known as "phase-reduction analysis". This method has been used to uncover some conditions for synchronization, such as the influence of periodic external forcing on an unsteady cylinder wake [6]. Additionally, we conduct research about this method to reveal conditions of the frequency lock-on within a network of oscillators.

The overall physics governing rhythmic systems can be too complex and high-dimensional to reveal oscillator characteristics directly. To simplify, we transform these equations into one-dimensional phase equations using the scalar phase of each oscillator, rather than considering the full state dynamics. This technique, known as "phase-reduction analysis", allows us to uncover how the amplitude and frequency of external forces can cause oscillators to Lock-in.

In the following sections, we present the phase-reduction analysis for multiple oscillators. Furthermore, we expand this analysis to perturbations in global coupling oscillators, where we measure how the phase of one oscillator is delayed by forces from others.

2. Application

2.1 Limit-cycle oscillator

The dynamics of the oscillator is described by an ordinary differential equation,

$$\frac{d}{dt}\mathbf{X}(t) = \mathbf{F}(\mathbf{X}) \quad (2.1)$$

where $\mathbf{X} = (X_1, X_2, \dots, X_M)$ is a real vector of a M-dimensional state space, t is time and $\mathbf{F}(\mathbf{X}) = (F_1(X), F_2(X), \dots, F_M(X))$ is the vector field of the oscillator dynamics.

In this report, we define this three-dimensional system of ordinary differential equations as oscillators,

$$\left. \begin{aligned} \dot{x} &= \mu x - \gamma y - \alpha x z - \beta x y \\ \dot{y} &= \gamma x + \mu y - \alpha y z + \beta x^2 \\ \dot{z} &= -\alpha z + \alpha(x^2 + y^2) \end{aligned} \right\} \quad (2.2)$$

where \dot{x} is dx/dt , and $\alpha, \gamma, \mu > 0$. This toy model shares some features with Navier-Stokes equations, such as energy conserving [7]. For Navier-Stokes equations, if $\langle \mathbf{u} \cdot \nabla \mathbf{u}, \mathbf{u} \rangle = 0$ is full field with typical boundary conditions on u , the nonlinear terms are energy conserving. For our toy model, the nonlinear terms $\mathbf{f}(x, y, z) = (-\alpha x z - \beta x y, -\alpha y z + \beta x^2, \alpha(x^2 + y^2))$ satisfy $\langle \mathbf{f}(\mathbf{q}), \mathbf{q} \rangle = 0$. In addition, we remark this system is closely related to the reduced-order model of the flow past a cylinder used by Noack *et al* [8], and the well-known Stuart-Landau model [9]. Next, we transform this model (2.2) to below equations

$$\left. \begin{aligned} \dot{r} &= (\mu - \alpha z)r \\ \dot{\theta} &= 1 + \beta r \cos \theta \\ \dot{z} &= \alpha(r^2 - z) \end{aligned} \right\} \quad (2.3)$$

According to these equations (2.3), we can find a limit cycle at $r^2 = z = \mu/\alpha$ in this dynamical system, which we

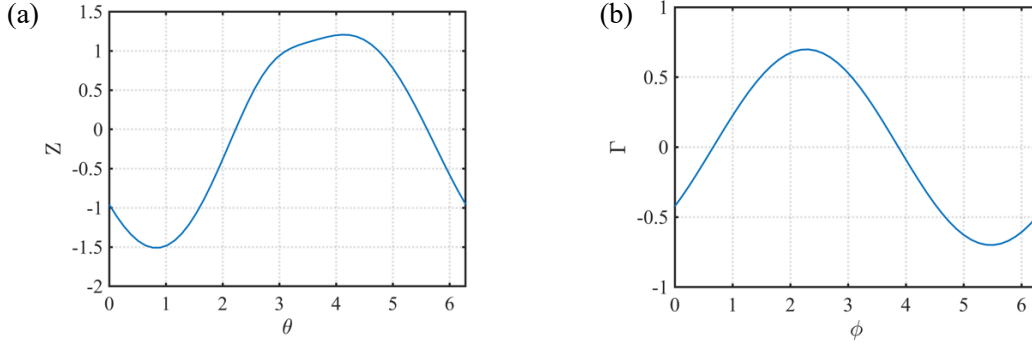


Figure 1 (a) “phase sensitivity function” is shown in order to the kicked phase’s change. (b) “phase coupling function” is shown in order to the phase difference’s change between oscillators and periodic perturbation.

denote by χ . In order to know the period T on the limit cycle, we calculate this integrating.

$$\int_{t_0}^{t_0+T} \dot{\theta} dt = 2\pi \quad (2.4)$$

$$T = \frac{2\pi}{\sqrt{1 - \frac{\beta^2 \mu}{\alpha}}} \quad (2.5)$$

Therefore, the natural frequency of the limit cycle is

$$\omega = \frac{2\pi}{T} = \sqrt{1 - \frac{\beta^2 \mu}{\alpha}} \quad (2.6)$$

where $\mathbf{X}_0(t + T) = \mathbf{X}_0(t)$ holds.

2.2 Phase sensitivity function

The limit-cycle oscillators are driven by external forcing or are mutually interacting. In phase reduction theory, the response function of the oscillator phase to external perturbation plays an important role, which we call simply “phase sensitivity function”.

We consider the situation that the oscillator is perturbed by a perturbed vector $\mathbf{I} = (I_1, I_2, \dots, I_M)$ on the limit cycle χ . Here, we define the “phase response function” $g(\theta; \mathbf{I})$ for characteristic of the response property of the oscillator phase to an external impulsive stimulus given at phase θ .

$$g(\theta; \mathbf{I}) = \Theta(\mathbf{X}_0(\theta) + \mathbf{I}) - \theta \quad (2.7)$$

where $\Theta(\mathbf{X})$ is the phase function in order to transform the oscillator state to its phase within the limit cycle χ . For this reason, we can figure out the new phase of oscillator after the perturbed vector by $\Theta(\mathbf{X}_0(\theta) + \mathbf{I})$.

We consider weakly perturbed oscillators. When the magnitude of \mathbf{I} is sufficiently small, this model can follow the linear-response framework and the phase function can be expanded in a Taylor series as

$$\begin{aligned} & \Theta(\mathbf{X}_0(\theta) + \mathbf{I}) \\ &= \Theta(\mathbf{X}_0(\theta)) + \nabla\Theta(\mathbf{X})|_{\mathbf{X}=\mathbf{X}_0(\theta)} \cdot \mathbf{I} + O(|\mathbf{I}|^2) \end{aligned} \quad (2.8)$$

where $\Theta(\mathbf{X}_0(\theta)) = \theta$. We can remake the phase response function with the expanded function (2.8) as

$$g(\theta; \mathbf{I}) \approx \nabla\Theta(\mathbf{X})|_{\mathbf{X}=\mathbf{X}_0(\theta)} \cdot \mathbf{I}. \quad (2.9)$$

We can define the “phase sensitivity function” [10], which gives a M -dimensional gradient vector of $\Theta(\mathbf{X})$ estimated at $\mathbf{X} = \mathbf{X}_0(\theta)$ with phase θ on the limit cycle χ as

$$\mathbf{Z}(\theta) = \nabla\Theta(\mathbf{X})|_{\mathbf{X}=\mathbf{X}_0(\theta)}. \quad (2.10)$$

According to this phase sensitivity function, we can see how the oscillator phase is advanced or delayed depending on the timing of the perturbation.

In our simulation we kick each component of oscillator state by a very weak impulse \mathbf{I} at some values of phase θ in order to obtain the “phase sensitivity function”.

$$\mathbf{Z}_j(\theta) = \lim_{I \rightarrow 0} \frac{g(\theta; I\mathbf{e}_j)}{I} \quad (2.11)$$

where \mathbf{e}_j is a unit vector along the j th component’s oscillator state.

We introduce small impulse to the 1st component’s oscillator state with our model (2.2). We measure the phase response function $g(\theta; I\mathbf{e}_x)$ directly (see Figure 1(a)). Then, this phase sensitivity function can be obtained in the principle (2.11) (see Figure 1(b)).

2.3 Periodic forcing

We consider controlling oscillator by adding a periodic force as

$$\frac{d}{dt}\mathbf{X}(t) = \mathbf{F}(\mathbf{X}) + \varepsilon\mathbf{f}(t) \quad (2.12)$$

where ε is a parameter representing the amplitude of external forcing and $\mathbf{f}(t)$ is the function to add external

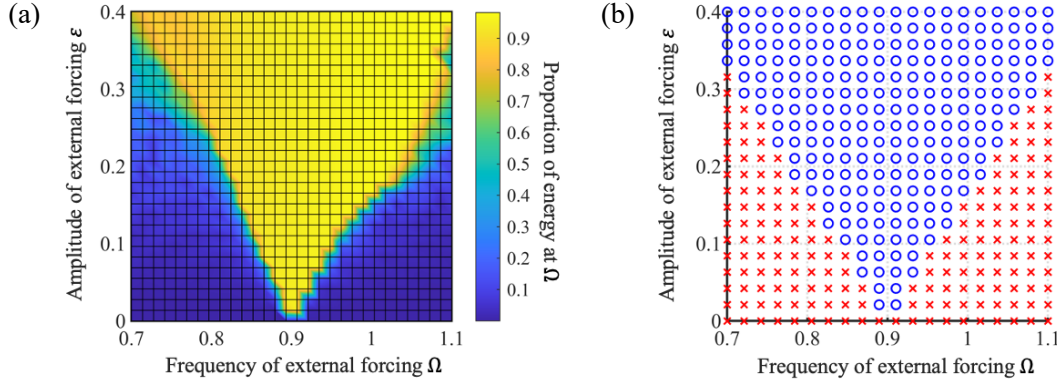


Figure 2 (a) The proportion of energy at frequency of periodic perturbation is shown for different forcing amplitude and frequency in terms of synchronization to periodic external forcing (b)Synchronized and unsynchronized cases are shown by o and x respectively, where the criterion for synchronization depends on inequality (2.17).

periodic force with $\|f\| = 1$. Here, ε should be enough significantly from the limit cycle χ of no external force case.

Now we can transform the phase equation with product raw as

$$\begin{aligned} \frac{d}{dt}\theta(t) &= \frac{d}{dt}\Theta(\mathbf{X}(t)) = \text{grad}_{\mathbf{X}}\Theta(\mathbf{X})|_{\mathbf{X}=\mathbf{X}(t)} \cdot \frac{d}{dt}\mathbf{X}(t) \\ &= \text{grad}_{\mathbf{X}}\Theta(\mathbf{X})|_{\mathbf{X}=\mathbf{X}(t)} \cdot \{\mathbf{F}(\mathbf{X}) + \varepsilon\mathbf{f}(t)\} \\ &= \omega + \varepsilon\mathbf{Z}(\theta) \cdot \mathbf{f}(t). \end{aligned} \quad (2.13)$$

Here, we define a periodic external forcing's $\mathbf{f}(t)$ frequency Ω and the difference between $\theta(t)$ and the frequency as

$$\phi(t) = \theta(t) - \Omega t. \quad (2.14)$$

Then, $\phi(t)$ is followed by the equation (2.13)

$$\begin{aligned} \frac{d}{dt}\phi(t) &= \omega + \varepsilon\mathbf{Z}(\phi(t) - \Omega t) \cdot \mathbf{f}(t) - \frac{d}{dt}\Omega t \\ &= (\omega - \Omega) + \varepsilon\mathbf{Z}(\phi(t) - \Omega t) \cdot \mathbf{f}(t) \\ &= \varepsilon\{\Delta + \mathbf{Z}(\phi(t) - \Omega t) \cdot \mathbf{f}(t)\} \end{aligned} \quad (2.15)$$

where Δ is the parameter depending on the frequency difference. We can assume that $\phi(t)$ isn't changed significantly within the period of external forcing T_{ext} by the approximation of integration as

$$\begin{aligned} \mathbf{Z}(\phi(t) - \Omega t) \cdot \mathbf{f}(t) &\approx \frac{1}{T_{\text{ext}}} \int_t^{t+T_{\text{ext}}} \mathbf{Z}(\phi(t') - \Omega t') \cdot \mathbf{f}(t') dt' \\ &= \frac{1}{2\pi} \int_0^{2\pi} \mathbf{Z}(\phi + \psi) \cdot \mathbf{f}\left(\frac{\psi}{\Omega}\right) d\psi. \end{aligned} \quad (2.16)$$

Here we define $\Gamma(\phi)$ as the “phase-coupling function” (see Figure 2(b)) with

$$\Gamma(\phi) = \frac{1}{2\pi} \int_0^{2\pi} \mathbf{Z}(\phi + \psi) \cdot \mathbf{f}\left(\frac{\psi}{\Omega}\right) d\psi. \quad (2.17)$$

With using (2.17), we can simplify the equation (2.15) as

$$\frac{d}{dt}\phi(t) = \varepsilon\{\Delta + \Gamma(\phi)\}. \quad (2.16)$$

If the “phase-coupling function” satisfied the following inequality

$$\varepsilon \min_{\phi} \Gamma(\phi) < \omega - \Omega < \varepsilon \max_{\phi} \Gamma(\phi), \quad (2.17)$$

the dynamics show stable behavior because there are at least two fixed points that $d\phi(t)/dt = 0$. We can see the region of stability over the $\Omega - \varepsilon$ space, known as the Arnold tongue [11]. We show the relationship in our model (2.2) (see Figure 2(a)).

3. Synchronization of coupled oscillators

3.1 Phase equation for coupled oscillators

In the previous section, we consider one dynamics of oscillators (2.1). Here we consider a system of N limit-cycle oscillators with interactive force. The dynamics of the i th oscillator state X_i ($i = 1, \dots, N$) are described by

$$\frac{d}{dt}\mathbf{X}_i(t) = \mathbf{F}_i(\mathbf{X}_i) + \sum_{j=1}^N \mathbf{A}_{ij}(\mathbf{X}_i, \mathbf{X}_j), \quad (3.1)$$

where $\mathbf{A}_{ij}(\mathbf{X}_i, \mathbf{X}_j)$ is a parameter which represent how big the interactive from the i th oscillator state to the j th one is and $\mathbf{F}_i(\mathbf{X}) = (\mathbf{F}_{i1}(\mathbf{X}_i), \mathbf{F}_{i2}(\mathbf{X}_i), \dots, \mathbf{F}_{iM}(\mathbf{X}_i))$ is the vector field of the i th oscillator dynamics individually. As follow the equations (2.13), we can obtain the j th phase equation for coupled oscillators with

$$\frac{d}{dt}\theta_i(t) = \frac{d}{dt}\Theta_i(\mathbf{X}_i(t)) = \text{grad}_{\mathbf{X}_i}\Theta_i(\mathbf{X}_i)|_{\mathbf{X}_i=\mathbf{X}_i(t)} \cdot \frac{d}{dt}\mathbf{X}_i(t)$$

$$\begin{aligned}
 &= \text{grad}_{\mathbf{X}_i} \theta_i(\mathbf{X}_i) |_{\mathbf{X}_i=\mathbf{X}_i(t)} \cdot \left\{ \mathbf{F}_i(\mathbf{X}_i) + \sum_{j=1}^N \mathbf{A}_{ij}(\mathbf{X}_i, \mathbf{X}_j) \right\} \\
 &= \omega_i + \mathbf{Z}_i(\theta_i) \cdot \sum_{j=1}^N \mathbf{A}_{ij}(\theta_i, \theta_j), \quad (3.2)
 \end{aligned}$$

where $\mathbf{A}_{ij}(\mathbf{X}_i(\theta_i), \mathbf{X}_j(\theta_j)) = \mathbf{A}_{ij}(\theta_i, \theta_j)$ and ω_i ($i = 1, \dots, N$) is the natural frequency of the i th oscillators. In addition, we can perform the averaging approximation, assuming that the effect of the mutual coupling is sufficiently small. We introduce new relative phase variables as follow

$$\phi_i(t) = \theta_i(t) - \Omega_{\text{rep}} t. \quad (3.3)$$

where Ω_{rep} is the representative frequency of the oscillator. Then, $\phi(t)$ is followed by the equation (3.2)

$$\begin{aligned}
 \frac{d}{dt} \phi_i(t) &= \omega_i - \Omega_{\text{rep}} + \\
 \mathbf{Z}_i(\phi_i + \Omega_{\text{rep}} t) \cdot \sum_{j=1}^N \mathbf{A}_{ij}(\phi_i + \Omega_{\text{rep}} t, \phi_j + \Omega_{\text{rep}} t). \quad (3.4)
 \end{aligned}$$

We consider the ‘‘phase coupling function’’ of the i th oscillator from the kick of j th oscillator over one period of the limit-cycle oscillation with

$$\Gamma_{ij}(\varphi) = \frac{1}{2\pi} \int_0^{2\pi} \mathbf{Z}_i(\psi + \varphi) \cdot \mathbf{A}_{ij}(\psi + \varphi, \psi) d\psi. \quad (3.5)$$

This averaged equation is given on the phase equations (3.2) by

$$\frac{d}{dt} \phi_i(t) = \omega_i - \Omega_{\text{rep}} + \sum_{j=1}^N \Gamma_{ij}(\phi_i - \phi_j) \quad (3.6)$$

$$\frac{d}{dt} \theta_i(t) = \omega_i + \sum_{j=1}^N \Gamma_{ij}(\theta_i - \theta_j). \quad (3.7)$$

When there are the fixed points that $d\phi_i/dt = 0$, the dynamics will show the stable state. Therefore, if the ‘‘phase coupling function’’ of all oscillators becomes stable, we can consider these dynamics are synchronized, which we call the ‘‘global coupling’’. If the ‘‘phase coupling functions’’ satisfied the inequality ($i = 1, \dots, N$)

$$\min_{\phi_i} \sum_{j=1}^N \Gamma_{ij}(\phi_i - \phi_j) < \omega_i - \Omega_{\text{rep}} < \max_{\phi_i} \sum_{j=1}^N \Gamma_{ij}(\phi_i - \phi_j), \quad (3.8)$$

which means we can select all relative phase ϕ_i ($i = 1, \dots, N$) and the representative frequency Ω_{rep} , these oscillators are ‘‘grovel coupling’’ around the frequency.

3.2 Interactive force on gaussian

In this section, we introduce the definition of interactive force $\mathbf{A}_{ij}(\mathbf{X}_i, \mathbf{X}_j)$ in our model under the dynamics (3.1) with

$$\mathbf{A}_{ij} = \begin{cases} a_i \frac{2}{\sqrt{\pi}} \exp \left\{ -\frac{\left(\frac{\omega_N - \omega_i - \frac{1}{2}}{\omega_N - \omega_1 - \frac{1}{2}} \right)^2}{c} \right\} \mathbf{X}_j \begin{bmatrix} 1 \\ 0 \end{bmatrix} & (i \neq j) \\ 0 & (i = j) \end{cases} \quad (3.9)$$

according to Gaussian function depend on their natural frequency ω_i , where $\omega_1 < \dots < \omega_i < \dots < \omega_N$ is required and a_i is the parameter of the influence between each oscillator and is defined at later section.

3.2.1 Same radius of the limit cycle

In this section, we consider the definition of model’s parameters $\alpha, \beta, \gamma, \mu$ (2.2) and the amplitude of interactive force a_i (3.9) on the same radius of limit cycle. First, this model takes $\gamma = 1$ without loss of generality. Form the equation (2.3), the radius of limit cycle depends on μ/a and the natural frequency depends on $\beta^2 \mu/a$. Therefore, after we chose ω_i ($i = 1, \dots, N$), $\mu = \mu_0$ and $\alpha = \alpha_0$, β_i ($i = 1, \dots, N$) will be decided automatically with

$$\beta_i = \sqrt{\frac{\alpha_0}{\mu_0(1 - \omega_i^2)}}. \quad (3.10)$$

In addition, it is fair that the influence of one oscillator to all is same as all of them. Under this logical, the interactive force \mathbf{A}_{ij} should be with

$$\sum_{j=1}^N |\overline{\mathbf{A}_{1j}}| = \dots = \sum_{j=1}^N |\overline{\mathbf{A}_{Nj}}| = \text{const}. \quad (3.11)$$

By this condition, if we choose the amplitude of interactive force a_k , the others a_i ($i \neq k$) is determined uniquely. Therefore, we choose the smallest amplitude of a_i ($i = 1, \dots, N$) at first, which is called the representative amplitude of interactive force a_0 , where a_i is represented as this function $a_i = h(a_0, i)$.

3.2.2 Different radius of the limit cycle

In this section, we reconsider the definition of model’s parameters $\alpha, \beta, \gamma, \mu$ (2.2) and the amplitude of interactive force a_i (3.9) on the different radius of limit cycle r_i with

$$r_i = \frac{b}{\omega_i^d}, \quad (3.12)$$

where b is the coefficient and d is the order to set the radius of limit cycle. The reason why we change the radius in this condition is for some dynamics to share this feature between the radius and frequency, such as law of conservation of angular momentum and energy cascade [12]. In this condition, the relationship (3.11) is should be satisfied. However, we assume that $|\overline{\mathbf{A}_{ij}}|$ depends on $|\mathbf{X}_i|$. That’s why this condition should be changed with

$$\frac{\sum_{j=1}^N |\overline{A_{1j}}|}{|\mathbf{X}_1|} = \dots = \frac{\sum_{j=1}^N |\overline{A_{Nj}}|}{|\mathbf{X}_N|} = \text{const.} \quad (3.12)$$

In addition, it is fair that the summation of all oscillators' radius is same as one of another set of oscillators when we want to compare one set of oscillators to another set, which has different order d . Under this logical, the interactive force A_{ij} should be with

$$\sum_{i=1}^N \sum_{j=1}^N |\overline{A_{ij}}| |r_j| = \text{const.} \quad (3.13)$$

3.2.3 Constant interactive of adjacent oscillators

In this section, we change the definition of gaussian parameter c in the interactive force, which is related to the width of gaussian. By condition of the equations (3.9), the width of gaussian depends on only parameter c . In the other hand, we want to change the width from the point of view that the interactive force between adjacent oscillators regardless of the number of N . We define the interactive force as

$$A_{ij}^* = \begin{cases} a_i \frac{2}{\sqrt{\pi}} \exp \left\{ -\frac{\left(\frac{\omega_N - \omega_i - \frac{1}{2}}{\omega_N - \omega_1 - \frac{1}{2}} \right)^2}{c^*(N-1)} \right\} \mathbf{X}_j \begin{bmatrix} 1 \\ 1 \\ 0 \end{bmatrix} & (i \neq j) \\ 0 & (i = j) \end{cases} \quad (3.14)$$

3.3 Periodic forcing to coupled oscillators

In this section, we add a periodic forcing to the k th oscillator in coupled oscillators designed by the model (3.1)

$$\begin{aligned} & \frac{d}{dt} \mathbf{X}_i(t) \\ = & \begin{cases} \mathbf{F}_i(\mathbf{X}_i) + \sum_{j=1}^N \mathbf{A}_{ij}(\mathbf{X}_i, \mathbf{X}_j) + \varepsilon \mathbf{f}(t) & (i = k) \\ \mathbf{F}_i(\mathbf{X}_i) + \sum_{j=1}^N \mathbf{A}_{ij}(\mathbf{X}_i, \mathbf{X}_j) & (i \neq k) \end{cases} \end{aligned} \quad (3.15)$$

As follow the equations (3.2), we can obtain the j th phase equation for coupled oscillators with

$$\begin{aligned} \frac{d}{dt} \theta_i(t) &= \frac{d}{dt} \Theta_i(\mathbf{X}_i(t)) = \text{grad}_{\mathbf{X}_i} \Theta_i(\mathbf{X}_i) |_{\mathbf{X}_i = \mathbf{X}_i(t)} \cdot \frac{d}{dt} \mathbf{X}_i(t) \\ &= \text{grad}_{\mathbf{X}_i} \Theta_i(\mathbf{X}_i) |_{\mathbf{X}_i = \mathbf{X}_i(t)} \cdot \left\{ \mathbf{F}_i(\mathbf{X}_i) + \sum_{j=1}^N \mathbf{A}_{ij}(\mathbf{X}_i, \mathbf{X}_j) + \varepsilon \mathbf{f}(t) \right\} \\ &= \omega_i + \mathbf{Z}_i(\theta_i) \cdot \sum_{j=1}^N \mathbf{A}_{ij}(\theta_i, \theta_j) + \mathbf{Z}_{ik}(\theta_k) \cdot \varepsilon \mathbf{f}(t), \end{aligned} \quad (3.16)$$

where $\mathbf{Z}_{jk}(\theta_k)$ ($i = 1, \dots, N$) is "phase sensitivity function" which is expanded to N limit-cycle oscillators from only one oscillator as follow

$$\begin{aligned} \mathbf{Z}_{ik}(\theta_k) &= \lim_{I_i \rightarrow 0} \frac{\Theta_i(\mathbf{X}_i(\theta_i) + \mathbf{I}_i) - \theta_i}{\mathbf{I}_i} \\ &= \lim_{I_i \rightarrow 0} \frac{\mathbf{g}_i(\theta_j; \mathbf{I} \mathbf{e}_j)}{I}. \end{aligned} \quad (3.17)$$

In our simulation, when we kick each component of k th oscillator state by a very weak impulse I at some values of phase θ_j , we measure the phase difference of i th oscillator $\mathbf{g}_i(\theta_k; \mathbf{I} \mathbf{e}_k)$ in order to obtain the "phase sensitivity function".

$$\phi_i(t) = \theta_i(t) - \Omega_{\text{ext}} t. \quad (3.18)$$

where Ω_{ext} is the frequency of the external forcing. Then, $\phi_i(t)$ is followed by the equation (3.16)

$$\begin{aligned} \frac{d}{dt} \phi_i(t) &= \omega_i - \Omega_{\text{ext}} + \\ & \mathbf{Z}_i(\phi_i + \Omega_{\text{ext}} t) \cdot \sum_{j=1}^N \mathbf{A}_{ij}(\phi_i + \Omega_{\text{ext}} t, \phi_j + \Omega_{\text{ext}} t) \\ & + \mathbf{Z}_{ik}(\phi_i + \Omega_{\text{ext}} t) \cdot \varepsilon \mathbf{f}(t). \end{aligned} \quad (3.19)$$

We consider the "phase coupling function" of the i th oscillator from the kick of j th oscillator over one period of the limit-cycle oscillation with

$$\Gamma_{ik}^*(\varphi) = \frac{1}{2\pi} \int_0^{2\pi} \mathbf{Z}_{ik}(\psi + \varphi) \cdot \varepsilon \mathbf{f} \left(\frac{\psi}{\Omega_{\text{ext}}} \right) d\psi. \quad (3.20)$$

This averaged equation is given on the phase equations (3.21) by

$$\frac{d}{dt} \phi_i(t) = \omega_i - \Omega_{\text{rep}} + \sum_{j=1}^N \Gamma_{ij}(\phi_i - \phi_j) + \Gamma_{ik}^*(\phi_i - \phi_k) \quad (3.21)$$

$$\frac{d}{dt} \theta_i(t) = \omega_i + \sum_{j=1}^N \Gamma_{ij}(\theta_i - \theta_j) + \Gamma_{ik}^*(\theta_i(t) - \theta_k(t)). \quad (3.22)$$

When there are the fixed points that $d\phi_i/dt = 0$, the dynamics will show the stable state. Therefore, if the "phase coupling function" of all oscillators becomes stable, we can consider these dynamics are synchronized, which we call the "global coupling". If the "phase coupling functions" satisfied the inequality ($i = 1, \dots, N$)

$$\begin{aligned} & \min_{\phi_i} \left\{ \sum_{j=1}^N \Gamma_{kj}(\phi_k - \phi_j) + \Gamma_{ik}^*(\phi_i - \phi_k) \right\} \\ & < \omega_i - \Omega_{\text{ext}} \\ & < \max_{\phi_i} \left\{ \sum_{j=1}^N \Gamma_{kj}(\phi_k - \phi_j) + \Gamma_{ik}^*(\phi_i - \phi_k) \right\}, \end{aligned} \quad (3.23)$$

which means we can select all relative phase ϕ_i ($i = 1, \dots, N$) and the frequency of the external forcing Ω_{rep} , these oscillators are "Lock-on" around the frequency.

4. Results

4.1 Same radius of the limit cycle

In this section we cast the result about same radius of the oscillator’s limit cycle, which is written in 3.2.1 section. Figure 4.1 is the difference of required interactive amplitude depending on the number of oscillators.

Figure 4.1 shows that wider Gaussian of the interactive force can make oscillators be same frequency easily than narrow one. Additionally, when we put more oscillators in the same range between ω_1 and ω_N , they can be global coupling much easily.

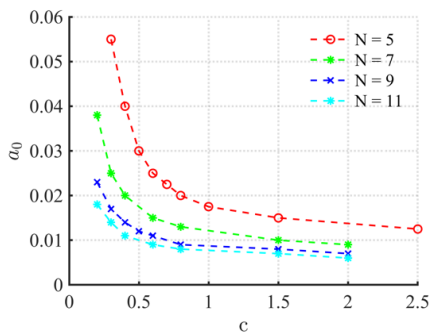


Figure 4.1 The required amplitude of interactive force to be global coupling based on width of Gaussian in the case of same radius of the limit cycle at the oscillator’s parameter $[\alpha, \gamma, \mu] = [0.2, 1.0, 0.2]$ and intrinsic frequency $[\omega_1, \omega_N] = [0.85, 0.9]$.

4.2 Different radius of the limit cycle

In this section we cast the result about different radius of the oscillator’s limit cycle, which is written in 3.2.2 section. Figure 4.2 is the difference of required interactive amplitude depending on the number of oscillators.

Figure 4.2 shows that wider Gaussian of the interactive force can make oscillators be same frequency easily than narrow one even in terms of high number of the order to set the radius of limit cycle. Additionally, the required amplitude in order to be global coupling decreased a little bit according to the order d .

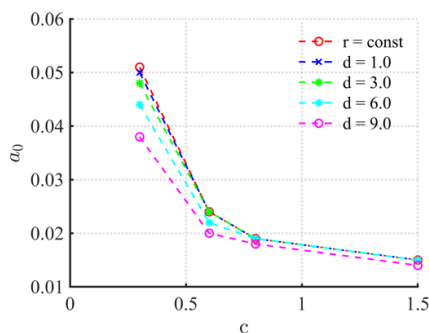


Figure 4.2 The required amplitude of interactive force to be global coupling based on width of Gaussian in the case of

same radius of the limit cycle at the oscillator’s parameter $[\alpha, \gamma] = [0.2, 1.0]$, intrinsic frequency $[\omega_1, \omega_N] = [0.85, 0.9]$ and $N = 9$.

4.3 Constant interactive of adjacent oscillators

In this section we cast the result about constant interactive of adjacent oscillators even if we change the number of oscillators, which is written in (3.14). Figure 4.3 is the difference of required interactive amplitude depending on the number of oscillators.

Figure 4.3 shows that wider Gaussian of the interactive force can make oscillators be same frequency easily than narrow one, which are same features as Figure 4.1. Additionally, all line is almost overlapped with each other.

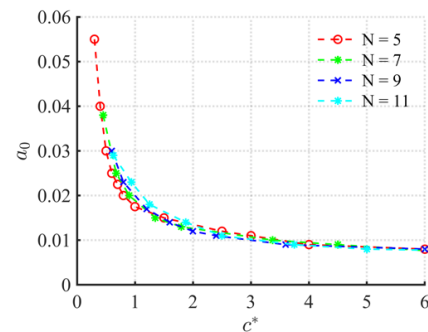


Figure 4.3 The required amplitude of interactive force to be global coupling cycle based on width of Gaussian (3.14) at the oscillator’s parameter $[\alpha, \gamma, \mu] = [0.2, 1.0, 0.2]$ and intrinsic frequency $[\omega_1, \omega_N] = [0.85, 0.9]$.

4.4 Estimation for global coupling

In this section, the required amplitude of interactive force to be global coupling is projected by “phase coupling function” (3.5). Figure 4.4 compares the actual required amplitude given in Figure 4.1 to the estimation in terms of standard deviation of their frequency.

Figure 4.4 shows that wider Gaussian of the interactive force and the higher amplitude of it can make the standard deviation be lower than narrow one in the same amplitude. Additionally, this colormap and the striped line which gives us the actual value is overlapped.

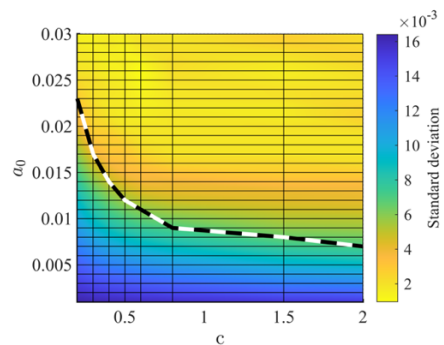


Figure 4.4 The estimation of required amplitude of interactive force is shown in colormap and the actual value

is written in striped line at the oscillator's parameter $[\alpha, \gamma, \mu] = [0.2, 1.0, 0.2]$, intrinsic frequency $[\omega_1, \omega_N] = [0.85, 0.9]$ and $N = 9$.

4.5 Lock-on by external forcing

In this section we cast the condition for Lock-on by periodic forcing into the oscillators, which are global coupling or not. Figure 4.5 compare the required amplitude for all oscillator to be same frequency as external perturbation in terms of the interactive amplitude's change.

Figure 4.5 shows that the case that the external perturbation is applied to near the center of oscillators makes them Lock-on by smaller amplitude of it than the edge. The oscillator's number which has the minimum required amplitude of external force increases according to the increasing power of external force. Compared to each figure, the oscillators which have high amplitude of interactive force are required high external forcing to be Lock-on.

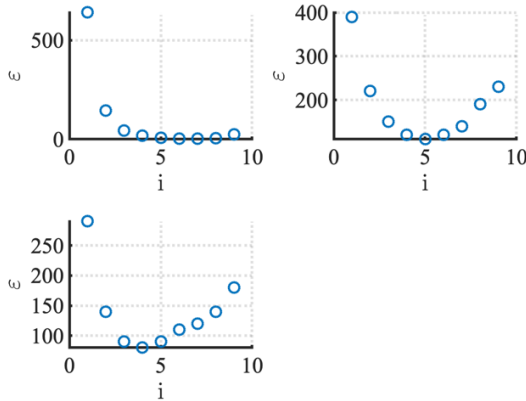


Figure 4.5 The estimation of required amplitude of external force in terms of the forced oscillator at the oscillator's parameter $[\alpha, \gamma, \mu] = [0.2, 1.0, 0.2]$, intrinsic frequency $[\omega_1, \omega_N] = [0.85, 0.9]$, $\Omega_{ext} = 0.865$ and $N = 9$. (a) The amplitude of interactive force $a_0 = 0.1$, where they are global coupling. (b) They are global coupling at $a_0 = 0.01$. (c) They aren't global coupling at $a_0 = 0.008$.

4.6 Estimation for Lock-on

In this section, the required amplitude of external periodic force to be Lock-on is projected by "phase coupling function" (3.5) and (3.20). Figure 4.6 compares the actual required amplitude given in Figure 4.5 to the estimation in terms of standard deviation of their frequency.

Figure 4.6 shows that the case that the external perturbation is applied to the 8th oscillators makes them Lock-on by smaller amplitude of it than the others.

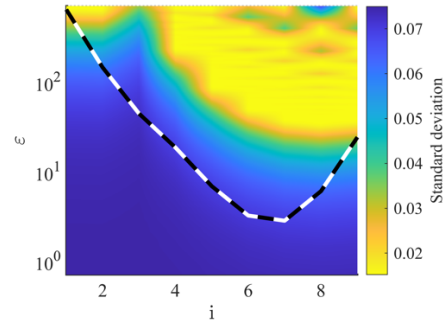


Figure 4.6 The estimation of required amplitude of external forcing is shown in colormap and the actual value is written in striped line at the oscillator's parameter $[\alpha, \gamma, \mu] = [0.2, 1.0, 0.2]$, $\Omega_{ext} = 0.865$, intrinsic frequency $[\omega_1, \omega_N] = [0.85, 0.9]$, $N = 9$ and $a_0 = 0.01$.

5. Discussion

5.1 Global coupling

Figure 4.1 shows that the required amplitude of interactive force for global coupling decreases with an increasing number of oscillators. However, Figure 4.3 demonstrates that if the number of oscillators is increased under the condition of interaction between adjacent oscillators, the required amplitude does not change significantly. Based on this result, we can infer that the relationship of forcing between adjacent oscillators plays the most crucial role in determining whether global coupling occurs. Figure 4.2 reveals that even when we change the radius of the limit-cycle according to their intrinsic frequency within a small range denoted by d , the essential amplitude does not change greatly.

The small standard deviation of oscillators' frequencies shown in Figure 4.4 indicates that these dynamics are close to global coupling because they have almost the same frequency. The actual value of the condition for global coupling is overlapped on the colormap around $s = 8 \times 10^{-3}$. This suggests that we can predict the correlation between the width of the Gaussian and the required amplitude for global coupling.

5.2 Lock-on case

Figure 4.5 shows that the oscillator with the minimum required amplitude of external force is located near the centre of all oscillators. We believe this result reveals that the oscillators around the centre have a significant influence on the others. If we aim to control multiple oscillators through perturbation, applying force to the central oscillator is very efficient.

In Figure 4.6, the estimation of the required amplitude of external forcing for Lock-on demonstrates that the edge oscillators require larger perturbations than the central one, which aligns with the actual values. However, there is an area with a larger standard deviation at the 3rd oscillator in the colormap.

6. Conclusion

- When the interactive force between each oscillator is applied to N oscillators along the Gaussian distribution, they can exhibit global coupling. If the Gaussian distribution of the interaction force has a wider width or higher amplitude, global coupling occurs more easily. The forcing relationship between adjacent oscillators plays a significant role in determining the conditions for global coupling, rather than the definition of the limit-cycle's radius and the number of oscillators.
- Expanding the "phase coupling function" from a single external perturbation to multiple interactive forces allows us to project the conditions regarding the amplitude and width of the interactive force.
- Expanding the 'phase sensitivity function' from one phase difference when an oscillator is kicked to one phase difference when another is kicked, allows us to roughly project the conditions regarding the amplitude and frequency of external periodic force. However, there are few differences between the actual conditions and the estimated values revealed by this analysis

- [10] Nakao, H. 2016 Phase reduction approach to synchronization of nonlinear oscillators. *Contemp. Phys.* 57 (2), 188-214.
- [11] Arnold, V. I. 1997 *Mathematical Methods of Classical Mechanics*. Springer
- [12] Alexandre J. Chorin, 1994, *Vorticity and Turbulence*, Applied Mathematical Sciences

ACKNOWLEDGEMENTS

Kaito Usami thanks Japan-US-Canada Advanced Collaborative Education Program (JUACEP, Nagoya University) to accomplish the visiting research at NCSU. I would also like to thank Prof. Chi-An Yeh and his group members for the insightful discussion and help about everything.

REFERENCES

- [1] A. Pikovsky, M. Rosenblum, and J. Kurths, *Synchronization: A Universal Concept in Nonlinear Sciences*, Cambridge University Press, Cambridge, 2001.
- [2] P.A. Tass, *Phase Resetting in Medicine and Biology: Stochastic Modeling and Data Analysis*, Springer, Berlin, 2007.
- [3] M. Rosenblum and A. Pikovsky, *Synchronization: from pendulum clocks to chaotic lasers and chemical oscillators*, *Contemp. Phys.* 44 (2003), pp. 401–416.
- [4] I. Aihara, Modeling synchronized calling behavior of Japanese tree frogs, *Phys. Rev. E* 80 (2009), p. 011918 1–7.
- [5] Phillip M. Munday, Kunihiko Taira, On the lock-on of vortex shedding to oscillatory action around a circular cylinder, *Physics of Fluids* 25, 013601 (2013)
- [6] Kunihiko Taira, Hiroya Nakao, Phase-response analysis of synchronization for periodic flows, *J. Fluid Mech* (2018), vol. 846, R2
- [7] Alberto Padovan, Samuel E. Ott and Clarence W. Rowley, Analysis of amplification mechanisms and cross-frequency interactions in nonlinear flows via the harmonic resolvent: *J. Fluid Mech.* (2020), vol. 900, A14,
- [8] Noack, B. R., Afanaiev, K., Morzynski, M., Tadmor, G & Thiele, F. 2003 A hierarchy of low-dimensional models for the transient and post-transient cylinder wake. *J. Fluid Mech.* 497, 335-363.
- [9] Stuart, J, T. 1958 On the non-linear mechanics of hydrodynamic stability. *J. Fluid Mech* 4, 1-21.

<3> Findings through JUACEP

3-1. Students' reviews ...P.32

3-2. Questionnaires (in Japanese) ...P.35

3-1. Students' reviews

Short Term Internship at Polytechnique Montréal

Name: Yu-Hsin Wu

Affiliation at Nagoya University: Department of Electrical Engineering

Participated program: Medium Course 2023

Research theme: Combinatorial Optimization for Geospatial Wind Turbine Placement

Advisor at the visiting university: Assist. Prof. Antoine Lesage-Landry

Affiliation at visiting university:

Department of Electrical Engineering, Polytechnique Montréal



During my exciting summer internship in Montreal, I was lucky to dive deep into a fascinating research project, exploring the intricate world of convex optimization. It was not just an academic endeavor; the city's vibrant cultures, languages, and cuisines turned it into a full-blown adventure.

I joined the team of brilliant minds I'd be collaborating with. Everyone was super welcoming, and my supervisor, Antoine, was a source of constant support and inspiration.

The project we were immersed in was challenging because it is the field outside of my major. We had dived into extensive literature reviews, collected and analyzed data, and engaged in heated discussions during our weekly meetings, bouncing ideas off each other. At first, formulation for the optimization problem was challenging for me because it requires many background knowledges and experience in the field. Since he led me a lot to break through the problem we had, I managed to get the hang of it.

I also picked up the skill to write program of convex optimization on Python, and I feel like my ability to analyze and understand the optimization has reached a whole new level. Collaborating with such a diverse team also taught me the importance of effective communication and the value of different perspectives.

Of course, it was not all about the work. Montreal, with its unique blend of English and French influences, was like a breath of fresh air. I found myself exploring the city's beauty and elegance, discovering artistic atmosphere in museums, diving into the local food scene, and hanging out with my friends at various cultural events and festivals. The multicultural vibe of the city was the cherry on top. Besides, the natural beauty surrounding the city and the nearby towns, each with its unique charm and vibe, were downright mesmerizing, offering a refreshing escape from the urban hustle when needed. The diverse atmospheres of each place added an extra layer of richness to my experience.

This internship was more than just a learning experience; it was a journey of personal and professional growth. I'm incredibly grateful to the whole team for welcoming me with open arms and for making this journey so memorable.

My wonderful stay in LA

Name: Koyo Ueno

Affiliation at Nagoya University: Department of Materials Chemistry

Participated program: Long course 2023-2024 (Sep 2023-Mar 2024)

Research theme:

Investigation of Ionic conductivity of Ionogel Electrolyte on separator

Pseudocapacitance of T-Nb₂O₅ Nanoparticles

Advisor at the visiting university: Prof. Bruce Dunn

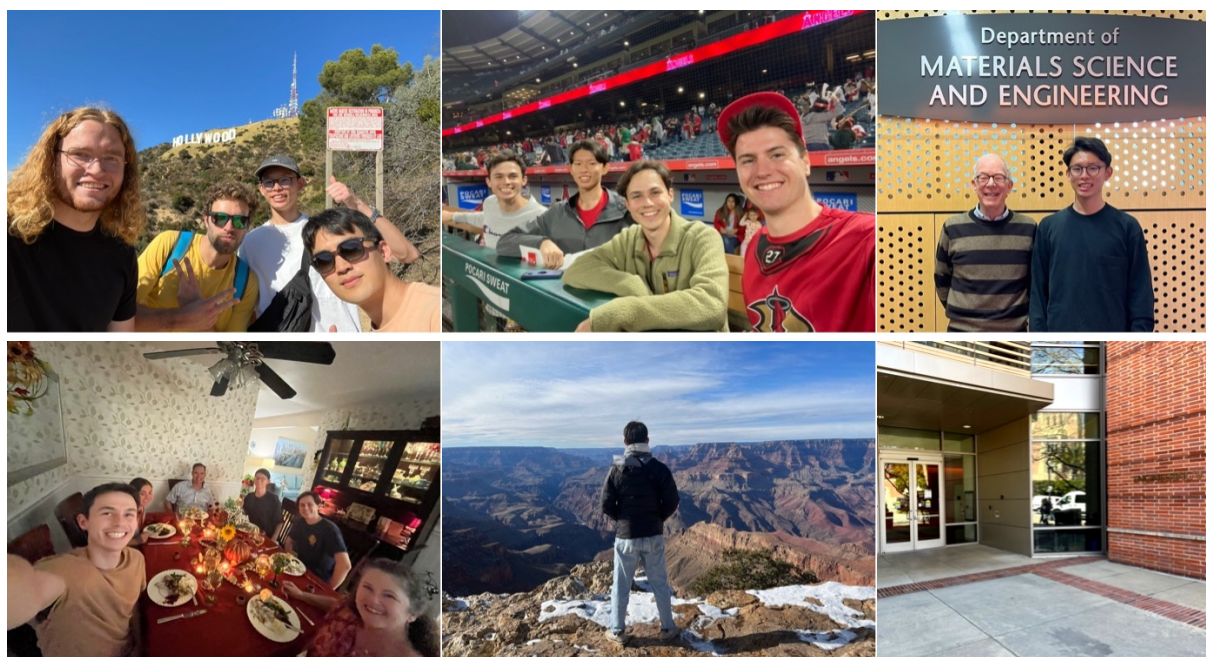
Affiliation at visiting university: Department of Material Science and Engineering, University of California, Los Angeles



These 7-months stay in LA were amazing. I am so happy to have had a great experience of not only research but also living in an environment that used to be unfamiliar to me. I tried wider variety of research than before by studying in different lab. I learned how students at UCLA work. What was most impressive was how friendly the people in my department were. When I had questions about my research, I often enjoyed discussing them with my lab members. Even when my English was not good, they tried to listen carefully and gently answered my question. Also, I broadened my knowledge by attending weekly seminars held for the department. Usually, a professor from other universities makes about an hour of presentation, and 30-40 students, researchers, and some faculties attend. At the beginning of my stay, I did not have the experience of listening to academic presentations in English so it was so difficult to understand. However, as I attended more times to the seminar, I learned to understand the talk and felt more confident.

Other than research, I enjoyed many “American” activities, including unique foods, watching sports, hiking, and gun shooting as well. I was so lucky to live with great roommates. I randomly found the apartment I lived in on Facebook. I had 5 roommates except me, and all of them are from California. I often hung out with them on weekends. Some of them are really interested in Japanese culture, especially Japanese food. We spent a lot of time eating dinner and talked about our different cultures. I also enjoyed the holiday activities. On Thanksgiving days, my roommates invited me to their family's house and we cooked a fancy dinner. Also, a church where my roommate and I sometimes went held a Christmas party. Throughout these activities, I learned American culture and improved my English.

Overall, I had great experiences with JUACEP program. This stay in the US changed my life in a good way. I strongly recommend people to challenge studying abroad and experience new things.



Findings through JUACEP in NCSU

Name: Katio Usami

Affiliation at Nagoya University: Dept. Aerospace Engineering

Participated program: Long-term course 2023

Research theme: Estimation for Multiple Oscillators' Global Coupling by Phase-Reduction Analysis

Advisor at the visiting university: Prof. Chi-An Yeh

Affiliation at visiting university: Dept. Mechanical and Aerospace Engineering, NCSU



1. In our laboratory

My visiting program was accepted by Prof. Chi-An Yeh. This group focuses on CFD, but my research at NU isn't related to it. That's why I was concerned about whether I could do it well or not before arriving. However, he supervised me and gave me an interesting research topic. I am enjoying conducting my research. We had weekly group meetings to explain and discuss our own research progress. I was gradually getting used to it. Apart from research, my colleagues always invited me to play table tennis, go to nightclubs, or eat out for fun. Additionally, when I was going through some problems and feeling down, they listened to me and encouraged me to go shopping to change my mood. I think the reason why I could have fun during my visit is that I like this group, and I am grateful to them.

2. In NCSU

I joined some clubs to gain experience, such as the English conversation club, cosplay club, Japanese culture club, and so on. During these activities, I met many people with diverse personalities and cultures and made some friends. I went to parties, shopping trips, concerts, and soccer games with them on weekends. In the international student's club, they invited us to celebrate Halloween, Thanksgiving, Christmas, and New Year's. I had valuable experiences that I couldn't have had in Japan.

3. Daily life in Raleigh

I lived in a share house with two people, a sibling pair consisting of an older sister and a younger brother from Afghanistan. Through this connection, I sometimes attended parties held by the Afghan community. The older sister would occasionally cook traditional Afghan dinners for us. In return, I made Japanese dishes, which I bought from Asian restaurants. This was the first time I had lived alone in my life, so every household chore was challenging for me. However, my cooking skills improved during this stay.

4. For travel

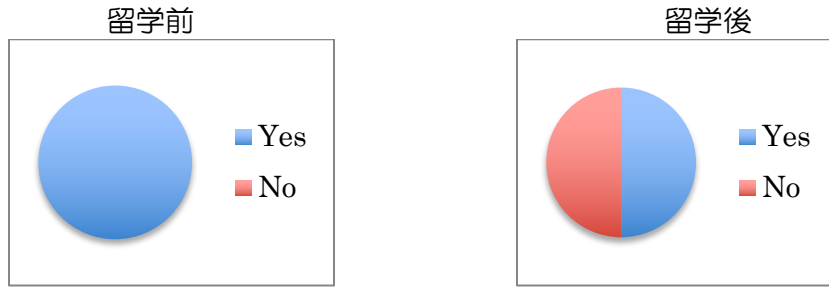
Watching the Ball Drop was on my bucket list, so I went to New York for the New Year's Eve of 2024. The night bus took a long time in such noisy conditions, and I had to stand in line to enter Times Square for ten hours, wearing diapers because once I left the line, I couldn't get back in. But it was definitely worth the wait. The sight of everyone there celebrating Happy New Year was spectacular, and I will always cherish that beautiful scenery in my heart.



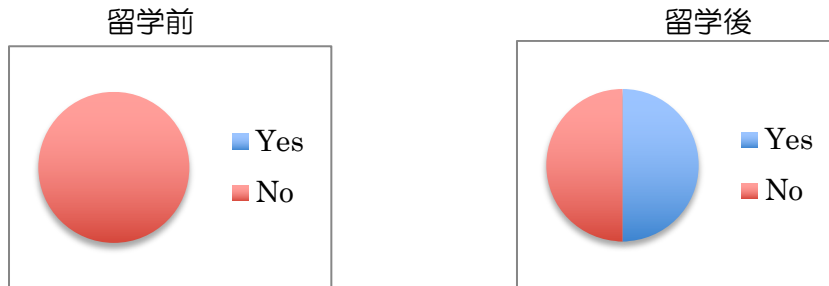
3-2. Questionnaires

派遣プログラム参加者に行ったアンケート結果

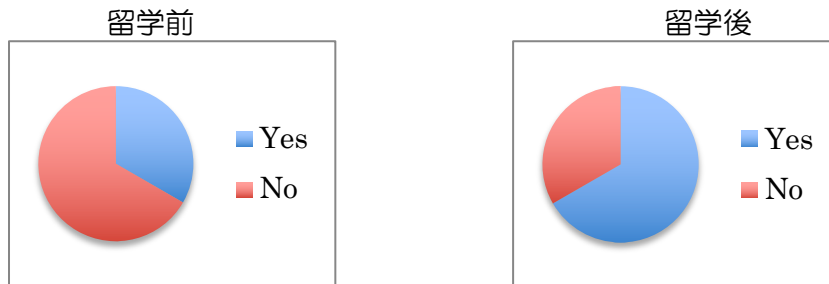
＜博士課程進学に興味がある＞



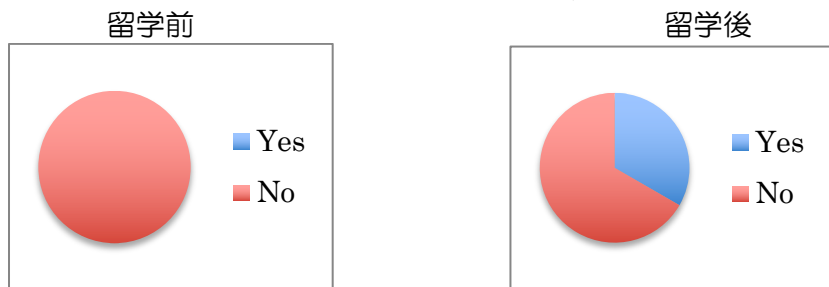
＜外国の大学での博士課程進学に興味がある＞



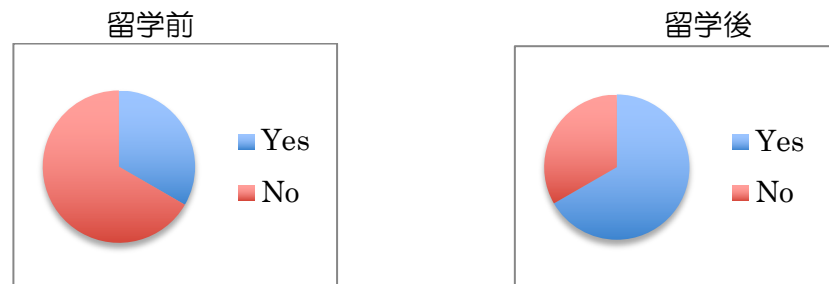
＜日本での外資系企業への就職に興味がある＞



＜外国での日系企業への就職（海外勤務）に興味がある＞



＜外国での日系以外の企業への就職に興味がある＞



アンケート結果まとめ 博士後期課程を目指す学生は国内で長年減少傾向だが、現地の研究チーム内で博士課程学生の役割・取組を目にして刺激を受け、外国での博士課程に興味を抱くようになる学生が毎年いる。現在は円安為替の影響で北米での自力生活が大変厳しいことを現地で経験し、日系企業への就職について影響が見られる。

3-2. Questionnaires

1. このプログラムの良かった点

- ・ 授業に縛られることがないので、研究に時間を費やすことができる。
- ・ オフィスが、留学準備のサポートをしてくれること。
- ・ ほぼ無条件で給付型奨学金が受給できる。
- ・ NCSUと名古屋大学が協定校であり、コーディネータから留学前に担当教授を探す際や留学中に支援をもらったこと。
- ・ このプログラムに参加することで、条件を満たせば単位が付与され、留年することなく、学年を進めることができる。
- ・ 事前ガイダンスなどがわかりやすく、フォローしやすいこと。奨学金サポートがあること。



2. このプログラムで改善してほしい点

- ・ 特にないが、無理に挙げるならば円安と物価高の影響で奨学金が不足しており、親の金銭的なサポートがなければ留学に行けなかった（プログラム側が改善できることではないと思うが）。
- ・ VISA申請、アパート探しなど分からないことだらけで心が折れそうになったので、もう少し詳しく教えて欲しかった。過去に留学した先輩ともっと話す機会があれば良いと思った。
- ・ 為替と物価のせいでかなり親に負担をかけたので金銭的な支援をもう少し頂けるとありがたかった。
- ・ 航空券の支給があればいい。



3. 住居について [A] 宿舎の見つけ方・宿舎形態・家賃・大学までの足 [B]感想

- ・ [A] インターネット。615CAD/月。大学までメトロで30分。
[B] 自分で探して契約するのでなく、留学先の大学から宿舎の提供（寮など）があったらいいと思う。
- ・ [A] FacebookにNCSUの学生のグループがあり、その中からシェアハウスを探した。900USD/月。大学までバスで15分。
[B] 南側は田舎で、北側が都会のイメージ。スーパーや飲食店などの店舗や主なバス停などは北側にあるのでそちらに宿を借りたほうが良い。自分は南側に借りたので、飲食店やバス停が遠かった。
- ・ [A] FacebookでUCLA Housingと検索するとグループがたくさん出てくる。詐欺っぽいものもあるので注意が必要だが、そのグループの投稿を見て連絡し、アパートを見つけた。800USD/月 光熱費込。大学まで徒歩15分。
[B] 家探しは渡米前の手続きで一番苦労した。詐欺対策のため最初の2週間ほどホテルをとって現地に行ってから探す方法もあるが、なるべく日本にいる間に済ませた方がいいと思う。Facebookやwebサイトで探す際には、ビデオ通話を繋げてもらって確認すると良い。また、LAの家賃はかなり高いの



3-2. Questionnaires

で、よほど金銭的に余裕がないとシェアハウスに住むのが前提になる。自分の肌感だと、double や triple だと\$1000 以下で収まるが、一人部屋が欲しいとなると\$1500 以上で、完全な一人暮らし（ワンルーム、studio）だと\$2000 以上だと思う。

4. 滞在中の印象深いことなど

- ・ 最初は楽しかったルームメイトとの生活が、文化の違いから少しずつストレスが溜まったこと。家族以外の人と一緒に生活することの難しさを知った。
- ・ 道路や家と家の間隔、大学のキャンパス、個室トイレなど何をとってもサイズが大きく土地の広大さを感じた。
- ・ キャッシュレス化が進んでおり、現金を使う機会がなかった。
- ・ 人が本当に親切でフレンドリーで、すごく助けてくれる。
- ・ とにかく天気が良く、ほぼ毎日快晴なので気分がいい。ただ、1日の寒暖差が結構あるので服装が少し難しい。
- ・ スーパーで肉とノートブックを買った時に会計後同じ袋に入れられて、ノートが肉汁でぐちゃぐちゃになった。amazon で頼んだものが置き配でぐちゃぐちゃの土の上に置かれた上、段ボールがボコボコになっていることがほぼ毎回だった。細かいことは気にしない文化。
- ・ 土地、建物、人、食べ物などすべてが大きくてびっくりする。特にキャンパスが古いがとても大きくきれいで驚いた。
- ・ テニスのプロが何度か大学に来て練習しており、UCLA の凄さを改めて実感した。



- ・ 街やトイレなど色々とあまり清潔ではない。おそらくアメリカ人はあまり気にしていないので受け入れるしかない。
- ・ モントリオール市内の大学は、同じWiFi システムを使っていて、自分の大学のアカウントで他の大学のキャンパス内でもWiFi が使える。学术交流活動などがある時や個人で環境を変えて勉強したい時など、ネット環境が共通だとすごく便利。

5. その他、自由コメント

- ・ この留学を通じて、本当に貴重な経験ができました。留学前も滞在中もサポートしていただいて本当にありがとうございました。今年以降で留学を考えている人がいれば自分にできるサポートをしたいと考えていますので、いつでも連絡してください。



Copyright © JUACEP 2024 All Rights Reserved

Published in October 2024

Japan-US-Canada Advanced Collaborative Education Program (JUACEP)

Graduate School of Engineering, Nagoya University

Furo-cho, Chikusa-ku, Nagoya 464-8603, Japan

committee@juacep.engg.nagoya-u.ac.jp

<https://www.juacep.engg.nagoya-u.ac.jp>